EXPERIMENTAL ANALYSIS OF RAINFALL-RUNOFF SAMPLING TECHNIQUES AND VOLUMETRIC CLARIFYING FILTER TREATMENT PROCESSES

By

CHRISTINA HERR

A THESIS PRESENTED TO THE GRADUATE SCHOOL
OF THE UNIVERSITY OF FLORIDA IN PARTIAL FULFILLMENT
OF THE REQUIREMENTS FOR THE DEGREE OF
MASTER OF ENGINEERING

UNIVERSITY OF FLORIDA

2011

To my wonderful fiancé Matt, my parents, my sister Jenny, and my grandma, who have always believed in me

ACKNOWLEDGMENTS

I would like to thank Dr. John J. Sansalone, who mentored me throughout the course of my graduate research. I would also like to thank Dr. Paul A. Chadik and Dr. Ben Koopman, who supported me by serving as members of my committee. Lastly, I would like to thank Hwan-Chul Cho, Josh Dickenson, Karl Seltzer, Hao Zhang, Greg Brenner, Aniela Burant, Moshik Doron, Jacqueline Martin, Adam Marquez, Julie Midgette, and Valerie Thorsen, who collaborated on fieldwork and laboratory analysis.

TABLE OF CONTENTS

page

LIST OF TABLES

LIST OF FIGURES

LIST OF ABBREVIATIONS

$A_{filter,\ s}$	surface area of filter (m^2)
A_s	surface area (m^2)
A_w	contributing area of the watershed (L^2)
b	cumulative power-law exponent based on particle diameter, dimensionless
BHS	baffled hydrodynamic separator
c	runoff coefficient (dimensionless)
$\bar{C}$	flow-weighted mean concentration of the constituent of interest for an event (g/L)
C_d	frictional drag coefficient (dimensionless)
CGD	cumulative gamma distribution
C_i	average concentration associated with period i (mg/L)
$C_{i\text{-}IN}$	mean influent concentration associated with sampling period i (mg/L)
$C_{j\text{-}EFF}$	mean effluent concentration associated with sampling period j (mg/L)
CWA	clean water act
d_p	diameter of a particle (m)
EMC	event mean concentration (mg/L)
EMV	event mean value
EPA	Environmental Protection Agency
g	gravitational acceleration (m/s^2)
h	rainfall depth (cm)
H_{calc}	calculated test statistic of the Kruskal-Wallis H test for significant difference
I_n	rainfall intensity of sample period n (L/s)
IPRT	initial pavement residence time (minutes)
K	total number of treatments in a Kruskal-Wallis H test

l	particle size parameter for the cumulative power law model
m	total number of effluent measurements taken during an event
M	total mass of the constituent of interest (g)
MBE	mass balance error (%)
ΣM_{eff}	cumulative mass load of the effluent across an entire event (g)
ΣM_{inf}	cumulative mass load of the influent across an entire event (g)
ΣM_{rec}	total mass of PM recovered after an event (g)
MS4	municipal separate storm sewer system
MTFR	maximum treatment flow rate (L/s)
n	total number of influent measurements taken during an event
N	particle number density for the cumulative-power-law model (count/m^3)
NPDES	National Pollutant Discharge Elimination System
NPS	non-point source
NRMSE	normalized root mean square error
NWS	National Weather Service
PDH	previous dry hours (hr)
PLM	power law model
PM	particulate matter
PND	particle number distribution (count/L)
PSD	particle size distribution (mg/L)
Q	volumetric flow rate (m^3/s)
QA/QC	quality assurance / quality control
Q_{max}	maximum volumetric flow rate (L/s)

Q_{mean}	mean volumetric flow rate (L/s)
Q_{med}	median volumetric flow rate (L/s)
Q_n	volumetric flow rate of sample period n (L/s)
R_d	particle Reynolds number (dimensionless)
r_i	the rank sum for treatment i
RMSE	root mean square error (mm)
RPD	ratio of prediction to deviation (dimensionless)
s	total number of data points in a Kruskal-Wallis H test
SD	standard deviation
SDV	standard deviation of the measured values in the prediction set
s_i	the number of samples in treatment i
SLR	surface loading rate ($L/min/m^2$)
SSC	suspended sediment concentration (mg/L)
SSE	sum of squared error
SOR	surface overflow rate (m/s)
TSS	total suspended solids (mg/L)
U_i	Mann-Whitney test statistic for treatment i
UOP	unit operations and processes
V	total volume of runoff in an event (L)
V_i	volume of flow during period i (L)
$V_{i\text{-}IN}$	volume of influent flow for sampling period i (L)
$V_{j\text{-}EFF}$	volume of effluent flow for sampling period j (L)
VCF	volumetric clarifying filter

V_s	particle settling velocity (m/s)
$V_{s,crit}$	critical settling velocity (m/s)
VSS	volatile suspended solids (mg/L)
$X_{1\,j}$	jth measurement of treatment 1
$\overline{X_1}$	mean of the measurements of treatment 1
$X_{2\,j}$	jth measurement of treatment 2
$\overline{X_2}$	mean of the measurements of treatment 2
x_{max}	maximum measured value of the manual sample PSD
α	power law index based on particle diameter (count/L^3)
β	cumulative power law exponent based on particle diameter (dimensionless)
k	shape factor of cumulative gamma distribution function
λ	scale factor of cumulative gamma distribution function
μ_f	fluid viscosity (g/m·s)
ρ_f	mass density of a fluid (g/m^3)
ρ_p	mass density of a particle (g/m^3)

Abstract of Thesis Presented to the Graduate School
of the University of Florida in Partial Fulfillment of the
Requirements for the Degree of Master of Engineering

EXPERIMENTAL ANALYSIS OF RAINFALL-RUNOFF SAMPLING TECHNIQUES AND VOLUMETRIC CLARIFYING FILTER TREATMENT PROCESSES

By

Christina Herr

August 2011

Chair: John J. Sansalone
Major: Environmental Engineering Sciences

Rainfall-runoff carries particulate matter (PM) from urban and agricultural land to surface waters and is the leading cause of impairment across all types of waterbodies. This impairment is partly due to the ecological impacts of PM on receiving waters and partly because many constituents of concern, like nutrients and metals, partition into these particles and are transported to surface waters in urban rainfall-runoff. It is crucial to accurately assess PM granulometry, mass load, and transport in order to select an effective unit operation to protect receiving waters from impairment.

One main objective of this study is to examine the hypothesis that a PM analysis based on manual sampling provides a more representative assessment of PM load and transport in urban rainfall-runoff for a small watershed than one based on peristaltic-pump-driven automated sampling. The other main objective is to examine the in-situ testing of a volumetric clarifying filter (VCF) treatment unit for the removal of PM and phosphorus from urban rainfall-runoff for a small watershed.

This study uses a series of paired manual grab samples and automated samples analyzed for suspended sediment concentration (SSC), particle size distribution (PSD), particle number distribution (PND), and PM fractions to compare the two sampling techniques. Tests for

significant difference (Kruskal-Wallis H test) are conducted on PSDs and PNDs. The cumulative gamma distribution (CGD) is used to model PSDs. Influent CGD parameters are significantly different ($p \leq \alpha = 0.05$) between sampling methods. PND results are modeled by the power law model (PLM). Neither influent nor effluent PLM parameters are significantly different ($p > \alpha = 0.05$) between sampling methods. Results indicate manual sampling is more appropriate for size heterodisperse PSDs. However, for size monodisperse effluent, as generated through primary clarification with or without filtration, with a relatively small median particle size, d_{50}, properly deployed automatic sampling can represent PSD and PND.

In order to assess the treatment potential of a VCF unit, field testing, including in-situ intra-event data collection and analysis of 25 actual rainfall-runoff events, is conducted on the unit. PM is separated into size fractions (sediment, settleable, and suspended PM; SSC) and quantified for both pre- and post- treatment samples. Laser diffraction is conducted to determine PSD. PM fractions are digested and analyzed for soluble reactive phosphorus (SRP) concentration. Results indicate that the VCF shows significant removal capabilities for both PM and particulate-bound P. The volume-weighted mean removal efficiency for total solids (in the form of SSC) is 98%, with the greatest removal coming from coarse particles (> 75 μm). Sediment-bound phosphorus is removed with the highest volume-weighted mean efficiency of 99% while the volume-weighted mean removal of total phosphorus is 68%. PM separation is divided into the two removal mechanisms utilized by the VCF, sedimentation and filtration to determine the relative contributions of each mechanism. Results indicate that removal of PM is significantly increased when filtration is utilized in addition to sedimentation.

CHAPTER 1
GLOBAL INTRODUCTION

Particulate matter (PM) from urban and agricultural land is conveyed to surface waters in rainfall-runoff. This is the leading cause of surface water impairment across all types of waterbodies (EPA, 2000). Impairment is due partly to the ecological impacts of PM on receiving waters and partly because many constituents of concern, like nutrients and metals, partition into these particles and are transported to surface waters in urban rainfall-runoff (Legret and Pagotto, 1999; Sansalone and Kim, 2008; Liu et al., 2010). It is crucial to accurately assess PM granulometry, mass load, and transport both because of impacts of the solids and particulate-bound constituents on receiving waters and because most stormwater treatment devices are assessed by their ability to remove these solids (Greb and Bannerman, 1997; Cristina et al., 2002; Sansalone and Kim, 2008).

One difficulty associated with stormwater sampling is choosing an appropriate sampling technique. The two most common techniques are manual grab sampling and automated sampling. Automated sampling is commonly used to sample rainfall-runoff for nonpoint source pollutants in small watersheds whereas manual sampling is more often used to sample larger streams and rivers. Automated samplers are often preferred in sampling projects because manual sampling can be more challenging. Manual grab sampling requires personnel to anticipate rainfall events, travel to the sampling site, and work in adverse weather conditions, all of which can be costly, time-consuming, and inconvenient (Harmel et al., 2003). However, studies have indicated that automated samplers used in rainfall-runoff monitoring are not capable of repeatedly capturing particles greater than 250 μm (Bent et al., 2001; Burton and Pitt, 2001; Clark et al., 2007). Using automated samplers in rainfall-runoff monitoring has the effect of misrepresenting PSDs, PM loads, and particulate-bound phosphorus loads and can potentially

lead to the improper selection and design of unit processes. Sampling technique is also critical in evaluating the treatment potential of stormwater unit operations and processes (UOPs). Only with an appropriate sampling technique can rainfall-runoff treatment technologies be assessed accurately.

A major challenge in stormwater management is selecting an appropriate rainfall-runoff treatment strategy. In many urban areas where there is limited area and high land cost, combined unit operations are preferred to individual treatment processes and large settling tanks (Grizzard et al., 1986). Baffled hydrodynamic separators (BHSs) have been favored in recent years for their small footprint (Wong et al., 1995; Walker et al., 1999); however, filtration unit operations have become more common for PM separation in rainfall-runoff (Liu et al., 2010). Selection of filtration unit operations depends on knowledge of PM load and granulometry, along with head-loss development and desired effluent water indices such as suspended sediment concentration (SSC), total suspended solids (TSS), and particle size distribution (PSD) (Clark, 2000). It is therefore critical to quantify and qualify the inputs to the unit and the outputs to receiving waters under a variety of rainfall intensities, runoff durations, and PM loads when evaluating the performance of a volumetric clarifying filter (VCF) unit.

CHAPTER 2
THE ROLE OF SAMPLING IN REPRESENTING RAINFALL-RUNOFF PARTICLE MATTER GRANULOMETRY

Introduction

Rainfall-runoff carries particulate matter (PM) from urban and agricultural land to lakes, streams, and rivers and is the leading cause of impairment across all types of waterbodies. In surface waters, the PM contained in surface runoff is a major constituent contributing to poor water quality (EPA, 2000). This is partly because particles can have ecological impacts on receiving waters and partly because many constituents of concern, like nutrients and metals, partition into the solid-phase and are transported to surface waters in urban rainfall-runoff (Legret and Pagotto, 1999; Sansalone and Kim, 2008; Liu et al., 2010). The partitioning of these constituents into PM in rainfall-runoff is highly affected by land use (e.g. transportation, recreation, and construction), particle size, and pollutant age (Liebens, 2001). It is therefore crucial to accurately assess PM granulometry as well as loads and transport in rainfall-runoff in order to select an effective unit operation or source control plan and to protect receiving surface waters from impairment (Greb and Bannerman, 1997; Cristina et al., 2002; Sansalone and Kim, 2008).

Currently, there are several difficulties associated with accurately assessing PM loads and transport in rainfall-runoff. One issue is choosing the PM index to be studied. There are two common gravimetric methods for quantifying PM: total suspended solids (TSS), Standard Methods 2540D (Standard Methods, 1995), and suspended sediment concentration (SSC), ASTM D3977-97 (Gray et al., 2000). Unfortunately both methods fail to give information about particle size distribution (PSD) and particle number distribution (PND). They only yield total mass load and mass concentration, which are insufficient for evaluating the behavior and maintenance of unit operations (Greg and Bannerman, 1997; Cristina et al., 2002). Additionally,

with the TSS method, a sub-sample is used for the analysis. Studies have shown that, for a sample containing a significant portion of coarse particles, defined as PM greater than 75 µm in diameter (ASTM, 2002; Rushton et al., 2007), the SSC method depicts a more accurate assessment of the total PM mass present in a sample (Grey et al., 2000; Clark and Siu, 2007). The aliquot taken for TSS is often not representative of the whole sample, which tends to underestimate the PM load of the whole sample and therefore underestimate the actual PM load of the runoff. On the contrary, the SSC method overcomes the challenge of taking a representative subsample by analyzing the entire volume. Therefore, if the sample is truly representative of the runoff, the SSC method is not affected by heterodispersity or the presence of sediment-size particles (> 75 µm) (Sansalone and Kim, 2008).

Another difficulty associated with accurately assessing PM loads is the selection of a sampling technique. There are two common sampling techniques: manual grab sampling and automated sampling. When sampling rainfall-runoff for nonpoint source pollutants in small watersheds, automated sampling is most commonly used, whereas manual grab sampling is more commonly used for larger streams and rivers (Harmel et al., 2003). Although automated samplers were originally developed for use in wastewater treatment, they are often preferred in stormwater sampling projects for small watersheds because the alternative, manual sampling, can be much more difficult. Manual grab sampling requires personnel to anticipate rainfall events, travel to the sampling site, and work in adverse weather conditions. This can be costly, time-consuming, and inconvenient (Harmel et al., 2003).

However, historically, stormwater monitoring studies utilizing automated samplers produce results that differ from those of studies using manual sampling (Sansalone et al., 1998; Furamai et al., 2002; Westerlund and Viklander, 2006). Currently, automated samplers used in

rainfall-runoff monitoring are not capable of repeatedly capturing particles greater than 250 µm. This is mainly due to lack of sufficient turbulence in pipes leading to a poorly-mixed water column (Bent et al., 2001; Burton and Pitt, 2001; Clark et al., 2007). Using automated sampling methods requires several assumptions to be made and, therefore, has several constraints. Automated sampling strategies typically assume that the entire watershed of interest is homogeneous and that water quality can be sampled at one intake point and be valid across the entire stream (Harmel et al., 2003). While this is usually the case with wastewater, it is often not with urban rainfall-runoff. Studies show that there are major differences between the PM of wastewater and that of urban rainfall-runoff (Furamai et al., 2002; Li et al., 2005). The PSD of typical wastewater is fine and size monodisperse. However, the PSD of typical urban rainfall-runoff is coarser and size heterodisperse with particles ranging from 1 to 10,000 microns in size (Li et al., 2005; Sansalone and Kim, 2008).

Although studies show that coarse PM is more easily removed from runoff than the suspended fraction, accurate information about this part of the gradation is important (Andral et al., 1999). A significant proportion of the total mass of constituents partitioning into the PM are associated with the sediment-size fraction. Studies show that more than 60 percent of particulate-bound metal mass (including Cd, Cu, Pb, and Zn) is associated with particles greater than 250 µm in diameter (Sansalone and Cristina, 2004). Furthermore, coarser fractions can significantly impact drainage systems conveyance capacity and runoff leaching in conveyance systems.

Objectives

The primary goal of this study is to examine the hypothesis that a PM analysis, based on manual grab sampling paired with the SSC method and PSD characterization, can provide a more representative assessment of PM load and transport in rainfall-runoff for a small watershed

than a PM analysis, based on peristaltic-pump-driven automated sampling paired with the SSC method and PSD characterization. The second objective is to identify for which particle sizes, if any, the results of the two sampling methods are significantly different. The third objective is to examine the hypothesis that although automated sampling may not provide representative results for PM load in size heterodisperse rainfall-runoff, representative results are produced for the size monodisperse treated effluent from a volumetric clarifying filter (VCF). This is based on a VCF which implements hydrodynamic separation and filtration and therefore produces effluent that does not contain any sediment-size particles.

Methodology

Unit Operations

This study utilizes two separate unit operations, a baffled hydrodynamic separator (BHS) and a VCF. The BHS unit used in this study is 1.2 meters in diameter and holds a volume of 1703 liters. It has a maximum treatment flow rate (MTFR) of 9.1 L/s. The system components include an inlet, an inlet drop pipe surrounded by a weir, an oil port, an outlet riser pipe, and an outlet. The vertical distance between the outlet pipe invert and the bottom of the base slab is 173 centimeters. The VCF unit is also 1.2 meters in diameter and is configured with two standard cartridges, each with a 70-millimeter-orifice cartridge lid, and one draindown cartridge with a 35-millimeter-orifice cartridge lid. Each cartridge contains eleven 20-micrometer filter tentacles made up of two 69-centimeter long segments. The system components include a 46-centimeter-diameter maintenance access pipe, a pressure relief pipe, a cartridge deck, a backwash pool weir located around the two standard cartridges, and a separator skirt. The unit has a MTFR of 12.6 L/s and is configured to begin bypassing flow when head loss reaches 46 centimeters. This is equivalent to a water elevation of 46 centimeters above the cartridge deck level.

Urban Source Area Watershed

The Reitz Union surface parking facility located on the University of Florida campus serves as the watershed in this study. Rainfall-runoff is collected from an existing stormdrain inlet at the southwest parking lot pavement edge as shown in Figure 2-1. The watershed is divided into two main sub-catchments, a parking area on the southeast side and an access road on the northwest side. Depending on the storm event, the watershed area ranges from 400 to 600 square meters with a median area of approximately 500 square meters. A butterfly valve is used at the inlet to prevent unwanted flow from entering the system. A 15-centimeter diameter PVC pipe carries runoff at a 6 percent slope from the inlet to a Parshall flume located 10 meters downstream. An ultrasonic sensor is fixed in the Parshall flume to record hydrology data. A 61 cm x 46 cm x 46 cm influent sampling drop box is located immediately downstream of the Parshall flume. A 15-centimeter diameter PVC tee-section carries the runoff from the outfall of the dropbox to the two treatment units. Diversion gate valves are used on each side of the tee to direct all of the influent to one of the two units. The VCF and the BHS are installed in parallel and a 61 cm x 46 cm x 46 cm effluent sampling drop box is located at each outfall.

There is an additional bypass pipe network for the VCF. It consists of a 15-centimeter diameter PVC pipe elevated to 122 centimeters above the unit's internal cartridge deck level, with a 5-centimeter diameter siphon break 30 centimeters above that. In the event that bypass occurs during an event treated by the VCF, untreated bypass effluent and treated effluent are sampled either as a composite or as two individual streams in the effluent sampling drop box. Bypass flow rate is measured with a 1-psi pressure transducer located in the bypass pipe. None of the events monitored for this study generated bypass.

Rainfall-Runoff Event-based Data Collection

Hydrology and PM data are collected for 8 events. Runoff samples are collected

using both manual grab sampling and automated sampling on a time basis using radar and observations made by physical inspection. The automated samplers used in this study are ISCO 3700 peristaltic-pump-driven automated samplers. Hydrology data are measured from an ultrasonic sensor located in the Parshall flume. Synchronized stop watches are used to record all sampling times and samples are volume-weighted based on these sampling times and paired flow rate measurements. Manual influent samples are taken in the influent sampling drop box. Manual effluent samples are taken in the effluent sampling drop box of the appropriate unit.

Automated influent samples are taken in one of two ways; for four of the monitored events, the influent automated sampling intake tube is located directly downstream of the inlet at the parking lot pavement edge. The intake tube is placed at the bottom of the pipe and oriented to face the flow head on. For the other four monitored events, the influent automated sampling intake tube is located in the outfall of the Parshall flume. The intake tube is placed in the vertical and horizontal center of flow, facing the flow. Automated effluent samples for all events are taken the same way. An effluent automated sampling intake tube is fed into the outlet pipe of each unit, the VCF and the BHS, and fixed along the bottom of the outlet pipe so as to face flow. Placing the automated sampler intake tube facing the flow and either locating it at the bottom of the flow or locating it at the center of flow are the two most common automated sampling collection methods recommended by manufacturers (Teledyne Isco, Inc., Lincoln, NE; American Sigma, Inc., Loveland, CO), required by regulators (EPA, 1992; Colorado Department of Public Health and Environment, 1996; State of Maine Bureau of Land and Water Quality Management, 2007), and ultimately selected for implementation (de Leon and Lowe, 2009; Reed, 1981).

Laboratory Analysis

After samples are collected, samples are transported directly back to the laboratory to be analyzed. Within the first 2 hours after the end of an event, turbidity measurements are taken on

each sample using a turbidimeter (Hach 2100AN Turbidimeter, ISO Method 7027). A 10-mL subsample is taken from the well-shaken 0.5 liter PSD samples for this turbidity measurement. Within the first 6 hours, laser diffraction is conducted using a laser diffraction particle analyzer (Malvern Instruments: Hydro 2000G) to determine PSDs from the 0.5 liter PSD samples. Prior to being poured into the analyzer, each sample is pre-screened with a #4 2000-µm sieve. This is done so that PM or other debris larger than 2000 µm is not allowed into the laser chamber. For each sample, the material collected in the #4 sieve is placed in a pre-weighed pan, dried in the oven at 105°C for 24 hours, and a final weight is recorded. Once samples are added to the wet chamber of the analyzer, multiple repetitions are required to reach stability across the entire gradation. The output from this instrument is in terms of percent finer by volume for each particle size ranging from 0.02 to 2000 µm. With paired SSC data (concentration and sample volume) from the remaining 0.5 liter samples, this output is converted to percent finer by mass.

SSC measurements are considered to be less time-sensitive than the PSD analysis and are conducted within 24 hours of the end of an event. 0.5 liter SSC samples are filtered through a 1 µm glass fiber filter with a vacuum pump. Filters are pre-washed with DI water, dried in a furnace at 550°C for 30 minutes, and weighed prior to use. The precise volume of each sample being filtered is also recorded. After filtering the samples, the filters and PM material captured by the filters are dried at 105°C. The final weights are recorded and the difference in dry weights is used to calculate the mass of PM and the SSC.

Data Analysis and Elaboration

Event mean concentration

While the inter-event distribution of PM is log-normal, a volume-weighted event mean concentration (EMC) is utilized as a comparative index for characterizing PM concentrations that

represent a flow-weighted PM concentration for a rainfall-runoff event (Sansalone and Kim, 2008). EMC is calculated using equation 2-1.

$$EMC = \frac{M}{V} = \overline{C} \tag{2-1}$$

In this expression, M represents the total mass of the constituent of interest (for example, SSC) over an entire event, V represents the total volume of runoff over that same event, and $\overline{C}$ represents the flow-weighted average concentration of the constituent of interest for an entire event.

Removal efficiency

While effluent concentrations provide a more physically-discernable measurement of treatment performance, a common comparative index for evaluating PM separation is percent removal. Percent removal is calculated using equation 2-2.

$$PR(\%) = \frac{\sum_{i=1}^{n}(V_{i-IN} \times C_{i-IN}) - \sum_{j=1}^{m}(V_{j-EFF} \times C_{j-EFF})}{\sum_{i=1}^{n}(V_{i-IN} \times C_{i-IN})} \times 100 \tag{2-2}$$

In this expression, $V_{i\text{-}IN}$ is the volume of influent flow for sampling period i; $V_{j\text{-}EFF}$ is the volume of effluent flow for sampling period j; $C_{i\text{-}IN}$ is the mean influent concentration associated with period i; $C_{j\text{-}EFF}$ is the mean effluent concentration associated with period j; n is the total number of influent measurements taken during an event; m is the total number of effluent measurements taken during an event.

Particle size distribution (PSD)

PSD is a primary measurement of PM granulometry. The output of the laser diffraction instrument is in percent finer by volume. A more common index is percent finer by mass, and

the commensurate indices of d_{10}, d_{50}, and d_{90} by mass. In order to make this conversion, the measured gravimetric mass (from SSC) is distributed over the entire PSD for each sample. Mass-based cumulative PSDs (i.e. percent finer by mass) for the samples are computed by integrating the gravimetric concentration of individual particle sizes for samples, corresponding flow rates, and sampling time intervals. With these paired data, PM total volume concentration for each particle size is converted to a gravimetric concentration in mg/L.

Cumulative gamma distribution

The PSDs are modeled gravimetrically using a cumulative gamma distribution (CGD). In order to represent any PSD both a dispersivity parameter and a representative parameter of PM size for the PSD are needed. The dispersivity parameter can be thought of as a characteristic of gradation uniformity or for example as a PM size sorting coefficient (Dickenson and Sansalone, 2009). Therefore a series of PSDs with the same representative PM size parameter but differing shapes can be generated. The PM size parameter is a representation of the fineness or coarseness of a PSD, for example a phi-scale (ϕ_n) particle size gradation parameter or more commonly a d_{50m}, where "m" indicates on a gravimetric basis (Dickenson and Sansalone, 2009). Modeling PSDs of differing uniformity and PM size representation is required for influent and effluent urban runoff. Previous studies (Sansalone and Ying, 2008; Lin et al., 2009) have utilized a two parameter CGD to model size heterodisperse PSDs. The shape and scale factor parameters in the CGD, k and λ, are physically analogous to the uniformity of the PSD and the representative coarseness or fineness of the PSD. Equations 2-3 and 2-4 represent the gamma distribution (*f(x)*) and CGD (*F(x)*), respectively.

$$f(x) = \frac{(x/\lambda)^{k-1} e^{(-x/\lambda)}}{\lambda \times \Gamma(k)} \qquad (2\text{-}3)$$

$$F(x) = \int_0^x f(x)dx \qquad (2\text{-}4)$$

In this expression x represents the particle diameter, d (μm), k represents a shape parameter, λ represents a scaling parameter and Γ(λ) is the gamma function.

Particle number density (PND)

While PM granulometry is most commonly measured and modeled based on common gravimetric size distributions (PSD and CGD), PM granulometry can also be examined based on particle number distribution (PND), the number of particles of a discrete size increment per a given volume of liquid. PND results are commonly modeled based on the assumption that PND can be represented by a truncated hyperbolic function, as a power law model (PLM) across a particle size range with details provided elsewhere (Bader, 1970; Cristina et al., 2002; Sansalone and Cristina, 2004). A similar presentation to PSD results can be made for PND, as percent finer by particle number. Following the determination of the cumulative PND, the distribution is modeled using a two-parameter PLM. The basic form of the PLM is summarized in the following expression and is plotted in a log-log domain to yield a linear representation of PND as a function of PM size across a truncated PSD.

$$\log(dN / d(d_p) = \log(\alpha) - \beta \log(d_p) \qquad (2\text{-}5)$$

In this expression N is the PND, d_p is the particle size parameter, and α and β are physically-based PLM parameters. To determine each parameter $\Delta N/\Delta d_p$ versus d_p is plotted with the intercept representing α and the slope representing β. As a gravimetric index of granulometry, PSD is dominated by the PM fraction of the gradation with the most mass, commonly the coarser PM, whereas PND as a number-based index of granulometry is dominated by the PM fraction of the gradation with the highest PM number, commonly the finest PM.

Kruskal-Wallis H test for significant difference

When comparing two or more sets of results that are not normally distributed, a useful test for significant difference is the Kruskal-Wallis H test. For this test, an H value is calculated and compared to a critical H value from the Chi Square Distribution. An H value is calculated by combining all the samples in the k treatments and ordering them from smallest to largest. Each sample is assigned a rank, with the smallest sample value being assigned first rank and the largest sample value being assigned nth rank. If any 2 or more data points are equal, each is assigned the average of the ranks. Next, the samples are divided into their original treatment groups and the ranks for each treatment are summed. An H value is then calculated using equation 2-6.

$$H_{calc} = \frac{12}{s(s+1)} \sum \frac{r_i^{\,2}}{s_i} - 3(s+1) \qquad (2\text{-}6)$$

In this expression, s is the total number of data points, r_i is the rank sum for treatment i, s_i is the number of samples in treatment i.

For the Kruskal-Wallis H tests conducted in this study, influent results are separated into two treatments, manual samples and automated samples. Effluent results are separated into four treatments, manual samples from the VCF, automated samples from the VCF, manual samples from the BHS, and automated samples from the BHS. For all tests, the null hypothesis (h_o) is that none of the treatments being tested are significantly different ($p > \alpha = 0.05$). The alternative hypothesis (h_a) is that at least two of the treatments being tested are significantly different ($p \leq \alpha = 0.05$). When the calculated H value exceeds the critical H value, χ^2_α, h_o is rejected and the conclusion is that at least two of the treatments are significantly different.

Normalized root mean square error

Normalized root mean square error (NRMSE) is another useful parameter in quantifying the difference between predicted values and measured values. In order to calculate NRMSE, it is necessary to first calculate the sum of squared error (SSE). SSE is calculated using equation 2-7.

$$SSE = \sum (x_{1j} - \bar{x}_1)^2 + \sum (x_{2j} - \bar{x}_2)^2 + \ldots \quad (2\text{-}7)$$

In this expression, x_{1j} is the jth measurement of treatment 1, $\bar{x}_1$ is the mean of the measurements of treatment 1, x_{2j} is the jth measurement of treatment 2, $\bar{x}_2$ is the mean of the measurements of treatment 2. RMSE is then calculated using equation 2-8.

$$RMSE = \sqrt{\frac{SSE}{n-k}} \quad (2\text{-}8)$$

In this expression, n is the total number of samples and k is the number of treatments.

RMSE is then normalized using equation 2-9.

$$NRMSE = RMSE \Big/ x_{\max} \quad (2\text{-}9)$$

In this expression x_{max} is the maximum measured value in the manual PSD distribution.

Newton's law

Settling velocity of a spherical particle in a fluid is calculated using Newton's Law provided in equation 2-10.

$$V_s = \sqrt{\frac{4g}{3C_d} \times \frac{\rho_p - \rho_f}{\rho_f} \times d_p} \quad (2\text{-}10)$$

In this expression, V_s is the settling velocity, g is the gravitational acceleration, ρ_p is the particle density, ρ_f is the fluid density, C_d is the frictional drag coefficient, and d_p is the particle diameter. C_d is calculated using equation 2-11.

$$C_d = \frac{24}{R_d} + \frac{3}{\sqrt{R_d}} + 0.44 \qquad (2\text{-}11)$$

In this expression, R_d is the particle Reynolds number.

Results and Discussion

The eight storms monitored in this study cover a wide range of rainfall intensities, runoff durations, and flow rates. Event duration ranges from 25 to 78 minutes. Rainfall depth ranges from 2.5 to 23.6 mm. Runoff volume ranges from 283 to 12010 liters. Peak flow rate ranges from 0.5 to 13 L/s and median flow rate ranges from 0.1 to 5 L/s. Event characteristics are shown in Table 2-1.

Measured SSC and PSD results for the eight events are included in Tables 2-2 and 2-3, respectively. PSD results of the 8 storms are pooled and Kruskal-Wallis H tests for significant difference are conducted on each PM size ranging from 0.02 to 2000 μm in diameter using the measured values of percent finer by mass for all samples. For the influent samples, there is no significant difference ($p > \alpha = 0.05$) between automated and manual samples for all particles smaller than 159 μm in diameter. However, for all particles larger than or equal to 159 μm in diameter, there is a significant difference ($p \leq \alpha = 0.05$) between automated samples and manual samples, indicating that although automated samplers accurately represent the fine fraction of particles, they fail to representatively capture particles larger than 159 μm in diameter. For the effluent samples, there is no significant difference ($p > \alpha = 0.05$) between automated samples and manual samples from the same unit operation, but there is a significant difference ($p \leq \alpha = 0.05$) between the PM separation provided by both the VCF and the BHS. This indicates that the automated sampler representatively captures particles across the entire PSD when it is size monodisperse and contains mostly fine particles. The significant differences between automated and manual PSDs for the 14 August event are illustrated in Figure 2-2. The influent and effluent

uncertainty bars in Figure 2-2 represent the standard deviation between all of the influent and effluent samples taken across the event.

In order to validate the manual sampling results and give meaning to the significant difference tests discussed above, the mass balance for PM of the BHS is determined using manual sampling results for influent and effluent as well as manual recovery of all PM separated by the BHS. The mass balance recovery is 95.1% with a mass balance error of 4.9% across the entire monitoring campaign. Therefore, results of manual sampling are taken as the representative influent and effluent values to which automated sampling results are compared. A statistically significant difference between results of the two sampling methods therefore indicates that results of automated sampling are significantly different from the actual representative PM results.

NRMSE is calculated for automated and manual PSDs. This is done for the difference in mass of each particle size in the PSD for automated and manual samples of all monitored events. NRMSE for influent PSD ranges from 0.11 to 0.30 with a volume-weighted mean of 0.13. NRMSE for effluent PSD from the BHS ranges from 0.09 to 0.60 with a volume-weighted mean of 0.50. NRMSE for effluent PSD from the VCF ranges from 0.09 to 0.99 with a volume-weighted mean of 0.28. NRMSEs are tabulated in Table 2-4. NRMSEs are relatively large for both influent and effluent PSDs, which indicates significant error between manual and automated PSDs. These results are consistent with those of the Kruskal-Wallis H test discussed previously.

In addition to NRMSE, PSD is modeled using a CGD. For this distribution, the PSD for each sample is modeled and a shape parameter, k, and a scaling parameter, λ determined. In the CGD, the shape parameter represents the uniformity of the PM size gradation and the scale parameter represents the coarseness of the PM. Influent k for manual samples ranges from 0.61

to 1.09 with a volume-weighted mean of 1.01. Influent k for automated samples ranges from 0.75 to 1.12 with a volume-weighted mean of 1.08. The higher volume-weighted k value for influent automated samples indicates that the distribution provided by automated samples is more uniform than that of manual samples and therefore contains a narrower range of particle sizes. This means that in failing to capture the large particles in a sample, the automated sampler is also failing to accurately assess the uniformity of particle sizes. Effluent k for manual samples from the BHS ranges from 0.86 to 1.25 with a volume-weighted mean of 1.21. Effluent k for automated samples from the BHS ranges from 0.83 to 1.15 with a volume-weighted mean of 1.12. Effluent k for manual samples from the VCF ranges from 0.66 to 1.35 with a volume-weighted mean of 1.25. Effluent k for automated samples from the VCF ranges from 0.55 to 1.34 with a volume-weighted mean of 0.99. Effluent automated and manual sample k values cover the same range of values and therefore do not appear to be different. This is because there are few to no coarse particles in the treated effluent of either unit and the automated sampler accurately represents the uniformity of particle sizes. Influent λ for manual samples ranges from 99.4 to 390 with a volume-weighted mean of 284. Influent λ for automated samples ranges from 146 to 268 with a volume-weighted mean of 229. The lower volume-weighted λ value of the automated samples indicates that the overall coarseness of particles is underrepresented by the automated sampler. Effluent λ for manual samples from the BHS ranges from 58.4 to 88.9 with a volume-weighted mean of 61.2. Effluent λ for automated samples from the BHS ranges from 83.8 to 133.5 with a volume-weighted mean of 92.8. Effluent λ for manual samples from the VCF ranges from 4.1 to 25.4 with a volume-weighted mean of 18.6. Effluent λ for automated samples from the VCF ranges from 5.0 to 36.8 with a volume-weighted mean of 28.6. As with the k values, the λ values for effluent automated and manual samples cover the same range of

values and therefore do not appear to be significantly different. CGD parameters for all events are shown in Table 2-5.

From these CGD results, Kruskal-Wallis H tests for significant difference are conducted on k and λ parameters for all samples. For the influent samples, there is a significant difference ($p \leq \alpha = 0.05$) between automated and manual samples for both k and λ. This is because the influent is size heterodisperse and contains coarse particles, and the automated sampler fails to accurately represent both the uniformity and coarseness of the PSD. For the effluent samples, there is no significant difference ($p > \alpha = 0.05$) for k and λ between any of the four treatments. This is because there are few coarse particles in the effluent and the automated sampler is able to accurately represent the uniformity and coarseness of the PSD. The significant differences between automated and manual k and λ parameters are illustrated in Figure 2-3.

In order to evaluate the role of the automated sampler intake tube's inner diameter in the significant difference between automated and manual samples at larger particle sizes, settling velocity is calculated for spherical particles ranging from diameter 0.02 to 2000 μm and compared to the uptake velocity of the automated sampler used in this study. Particles are assumed to be spherical in shape and a median particle density of 2.45 g/cm^3 is applied from previously measured data. In addition, the uptake velocity is calculated using an average measured flow rate and a 1-cm inner tubing diameter. The uptake velocity of the automated sampler tubing is 468 mm/s. The settling velocity of a spherical particle with diameter 159 μm is approximately 26 mm/s. The uptake velocity of the automated sampler is an order of magnitude higher than the settling velocity of a 159-μm particle, but the sampler still fails to repeatedly capture particles greater than or equal to this diameter. This demonstrates that the

significant difference between automated and manual samples containing particles at or above 159 μm in diameter cannot be attributed to intake tube selection alone.

In addition to PSD, PND is an important granulometric index of PM. Particle number indices d_{10}, d_{50}, and d_{90} (by number) for the eight events monitored in this study are shown in Table 2-6. From these results, Kruskal-Wallis H tests for significant difference are conducted on each particle size ranging from 0.02 to 2000 μm in diameter using the measured values of percent finer by number for all samples. For both influent and effluent PNDs, there is no significant difference ($p > \alpha = 0.05$) between automated samples and manual samples in terms of number of particles of each particle size between 0.02 and 2000 μm in diameter. This is because although coarse particles contain more mass than fine particles and dominate the PSD, fine particles are more plentiful than coarse particles and dominate the PND. Therefore, since the automated sampler accurately represents the fine fraction, it also accurately represents the PND.

The PND for each sample is modeled using a cumulative PLM. The PLM is applied only to particles ranging from 0.02 to 75 μm in diameter (fine fraction). This range is chosen because the fine fraction dominates the PND and for all storms, at least 99.98% of all particles by number are finer than 75 μm. For the PLM, the PND for each sample is linearly regressed with a slope of $-\beta$ and a y-intercept of α. The slope represents the dominant particle fraction, where a steeper slope indicates a preference for large particles and a flatter slope indicates a preference for small particles. The y-intercept represents the variability of particle concentration. For the comparisons between automated and manual samples for both influent and effluent, all of the PLM parameters are fairly consistent and generally have the same range of values for the two sampling methods. PLM parameter results for all events are shown in Table 2-7.

From these PLM results, Kruskal-Wallis H tests for significant difference are conducted on α and β parameters for all samples. For the influent samples, there is no significant difference ($p > \alpha = 0.05$) between automated and manual samples for both α and β. This indicates that the automated sampler accurately represents the total number of particles in a sample and the dominance of fine particles in that count. For the effluent samples, there is also no significant difference ($p > \alpha = 0.05$) between automated and manual samples from the same unit operation for α and β. Automated and manual PLM parameters are illustrated in Figure 2-4.

A Note about the Relationship between PND and Turbidity

Turbidity is a measure of the scattering of light by suspended particles (<75 µm). It significantly impacts the filtration and disinfection of surface waters. Therefore, the turbidity of a water sample is an important water quality characteristic to determine. Since both turbidity and PND are heavily influenced by fine particles, the measured values of percent finer by number for a variety of particle sizes between 0.02 and 75 µm for a set of samples are plotted with paired turbidity measurements, taken with a turbidimeter. Linear regressions for turbidity as a function of PND, in the form of percent finer by number, showed that the highest correlation between turbidity and PND occurs at a nominal 1-µm particle size. This indicates that not only is 1 µm the average d_{50} by number, but it is also the particle size that is most highly correlated to turbidity. The relationship between turbidity and the percent of particles finer than 1 µm by number is illustrated in Figure 2-5. Additionally, the coefficient of determination, r^2, between percent finer by number and turbidity increases with increasing particle size from 0.02 to 1 µm, peaks at about 1 µm, and then decreases with increasing particle size until it levels off from 1 to 75 µm. This is also shown in Figure 2-5.

PND and PSD both play an integral part in characterizing rainfall-runoff. The PSD provides information about how the mass of PM is distributed which is important for the fate and transport of nutrients and metals. The PND provides information about how the number of particles is distributed which is important for the quantification of cyst organisms. Sediment-size particles represent a large amount of the total mass and therefore tend to largely affect the PSD. However, they do not represent a large number of the total count and therefore do not tend to largely affect the PND. Fine particles represent a large number of the total count and therefore tend to largely affect PND. However, they do not represent a large amount of the total mass and therefore do not tend to largely affect the PSD. Hence, it is expected that PSD is more affected by automated sampling than PND, since automated sampling mainly impacts the collection of larger particles. This is illustrated in Figure 2-6, in which manual and automated influent PSDs and PNDs for the 13 August 2010 event and the 23 August 2010 event are plotted together. For the 13 August 2010 event, the manual influent d_{50} by mass is 182 µm and the automated influent d_{50} by mass is 117 µm. However, the manual influent d_{50} by number is 0.9 µm and the automated influent d_{50} by number is 0.5 µm. For the 23 August 2010 event, the manual influent d_{50} by mass is 190 µm and the automated influent d_{50} by mass is 120 µm. However, the manual influent d_{50} by number is 0.9 µm and the automated influent d_{50} by number is 0.7 µm.

There are significant differences ($p \leq \alpha = 0.05$) between samples taken manually and samples taken with an automated sampler. The finest particles have the smallest difference in percent finer by mass, but as particle size increases, so does this difference. A turning point occurs in the size gradation at 159-µm, when this difference becomes statistically significantly different. Figure 2-7 illustrates the increasing difference between the critical H value, χ^2_α and the calculated H value of the Kruskal-Wallis H test for PSD with increasing particle size. These

results indicate that the critical particle diameter at which there is a significant difference between manual sampling and automated sampling is 159 µm. This implies that for any size monodisperse treated effluent, like that of the VCF, with a d_{50} below 159 µm, there is no significant difference ($p > \alpha = 0.05$) between paired automated and manual samples. However, for any size heterodisperse influent, like that of typical urban rainfall-runoff there is a significant difference ($p \leq \alpha = 0.05$) between paired automated and manual samples.

Conclusions

This study examines manual and automated sampling results generated through paired sampling and analysis for PSD, PND, SSC and PM fractions. Results are based on eight runoff events captured from an urban source area in Gainesville, Florida. Whole sample fractionation is utilized for SSC and PM fractions, and laser diffraction for PSD and PND. Influent and effluent sampling for four events is examined for a VCF (primary sedimentation and filtration) and the additional four events for a BHS providing only primary sedimentation. Non-parametric testing is utilized to compare sampling methods for influent and effluent. Based on this framework of testing and analysis results illustrate that there are statistically significant differences between event-based manual grab sampling and automated sampling for influent SSC and PSD. While there is no significant difference between the two PND characterizations for size heterodisperse runoff with a d_{50} (by mass) at or above 159 µm, there is a significant difference between the two PSD characterizations. This indicates that manual grab sampling paired with the SSC method and PSD characterization is a more accurate PM analysis for most untreated urban rainfall-runoff from small watersheds.

However, for runoff containing mostly fine particles, this is not the case. For size monodisperse runoff with a d_{50} (by mass) below 159 µm, there is no significant difference between the two PM analyses. This indicates that either technique, if used appropriately,

provides a representative PM characterization of treated effluent from a unit implementing primary sedimentation as well as filtration. A preliminary PM analysis is required in this case to determine if the effluent is truly size monodisperse and composed of fine particles smaller than 159 μm.

There are two main constraints of automated samplers that are responsible for the difficulties associated with stormwater monitoring. The first is that they do not sample the entire depth of flow. The location of the intake tube within the depth of flow greatly impacts sampling, since higher concentrations of particles are found at lower depths. The second is that the uptake velocity of the automated sampler is usually not equal to the localized streamflow velocity. Runoff flow rates are not constant; however intake tube uptake velocities are fixed. This leads to mostly non-isokinetic sampling and substantial error due to inertial effects of the particles.

Table 2-1. Monitored rainfall-runoff event characteristics.

Event Date (2010)	PDH (hr)	Event duration (min)	Rainfall depth (mm)	Runoff volume (L)	Peak flow (L/s)	Median flow (L/s)	Mean flow (L/s)
31-July	72	60	23.6	9019	13.26	0.60	2.50
13-August	144	25	2.79	309	3.21	0.06	0.21
14-August	28	31	2.54	594	2.47	0.25	0.38
21-August	168	31	2.79	283	1.46	0.03	0.16
1-August	24	36	30.0	12007	13.26	4.74	5.49
7-August	24	48	8.64	2757	13.26	0.23	0.73
23-August	48	42	2.79	312	1.25	0.01	0.12
26-September	40	78	3.56	1129	0.45	0.26	0.24

The line separating the first set of events and the second set of events represents the breakpoint between the BHS events (top) and the VCF events (bottom).

Table 2-2. Summary of event-based PM fractions.

Event Date (2010)		PM < 75 µm [mg/L]		PM < 1000 µm [mg/L]		PM < 2000 µm [mg/L]		PM > 2000 µm [mg/L]		SSC [mg/L]	
		Manual	Auto	Manual	Auto	Manual	Auto	Manual	Auto	Manual	Auto
31-July	Influent	9.2	14.5	61.0	93.9	81.0	121.6	11.6	7.0	92.7	128.6
	Effluent	9.7	14.6	38.8	67.9	47.0	83.9	0.0	0.0	47.0	83.9
13-August	Influent	33.3	52.9	190.6	311.6	258.2	408.9	356.2	61.3	614.4	470.2
	Effluent	4.0	4.0	12.8	14.8	15.3	17.8	0.0	0.0	15.3	17.8
14-August	Influent	24.2	19.0	198.6	102.1	282.7	131.0	52.4	10.3	335.1	141.3
	Effluent	4.1	4.1	14.4	14.9	17.3	18.1	0.0	0.0	17.3	18.1
21-August	Influent	69.2	84.5	368.2	414.5	477.6	539.9	57.3	77.4	534.9	617.3
	Effluent	3.3	3.3	10.0	13.9	12.0	17.0	0.0	0.0	12.0	17.0
1-August	Influent	32.4	23.9	183.6	129.7	245.1	168.6	0.0	0.0	245.1	168.7
	Effluent	2.8	3.5	6.6	8.6	7.6	10.0	0.0	0.0	7.6	10.0
7-August	Influent	8.7	29.1	60.7	185.7	82.7	242.6	34.4	27.1	117.1	269.7
	Effluent	6.5	6.2	12.4	11.8	13.9	13.2	0.0	0.0	13.9	13.2
23-August	Influent	24.7	40.2	155.1	224.5	210.5	292.3	345.3	37.6	555.8	329.9
	Effluent	1.9	8.5	4.1	15.1	4.7	16.9	0.0	0.0	4.7	16.9
26-September	Influent	17.4	9.1	89.9	36.1	114.4	44.4	3.5	0.0	117.9	44.4
	Effluent	1.3	5.2	2.6	9.9	2.9	11.2	2.1	0.0	5.0	11.2

Influent and effluent refer to untreated and treated rainfall-runoff, respectively. The line separating the first set of events and the second set of events represents the breakpoint between the BHS events (top) and the VCF events (bottom).

Table 2-3. Summary of event-based PM indices of d_{10}, d_{50}, and d_{90}.

Event Date (2010)		PSD (μm) d_{10}		d_{50}		d_{90}	
		Manual	Auto	Manual	Auto	Manual	Auto
31-July	Influent	23.0	16.3	150.1	110.1	442.8	180.1
	Effluent	6.5	8.8	40.4	69.4	124.3	205.3
13-August	Influent	16.3	16.6	181.5	117.2	764.5	407.2
	Effluent	4.4	5.7	31.9	41.3	145.5	174.6
14-August	Influent	24.5	12.3	177.4	101.2	727.4	409.8
	Effluent	5.7	6.0	46.0	46.3	233.2	199.7
21-August	Influent	5.9	8.7	80.4	88.5	552.7	300.9
	Effluent	4.6	8.6	33.5	77.7	224.3	203.6
1-August	Influent	23.9	26.1	199.2	185.7	531.0	523.9
	Effluent	1.5	1.5	5.5	8.3	17.1	39.3
7-August	Influent	18.6	19.3	186.2	147.7	737.3	407.2
	Effluent	0.9	0.9	3.5	3.7	11.8	13.2
23-August	Influent	13.7	13.5	190.4	119.7	713.7	464.3
	Effluent	1.5	1.4	3.9	2.4	40.4	4.3
26-September	Influent	3.6	4.7	34.6	76.9	173.2	230.6
	Effluent	1.0	1.1	3.1	4.3	55.5	13.3

Influent and effluent refer to untreated and treated rainfall-runoff, respectively. The line separating the first set of events and the second set of events represents the breakpoint between the BHS events (top) and the VCF events (bottom).

Table 2-4. NRMSE between the incremental mass of automated samples and manual samples at each particle size across the PSD.

Event Date (2010)	PSD NRMSE	
	Influent	Effluent
31-July	0.135	0.534
13-August	0.194	0.093
14-August	0.301	0.091
21-August	0.300	0.599
1-August	0.113	0.286
7-August	0.114	0.091
23-August	0.274	0.990
26-September	0.191	0.498

Influent and effluent refer to untreated and treated rainfall-runoff, respectively. The line separating the first set of events and the second set of events represents the breakpoint between the BHS events (top) and the VCF events (bottom).

Table 2-5. Summary of event-based cumulative gamma distribution parameters for PSD.

Event Date (2010)		k		λ	
		Manual	Auto	Manual	Auto
31-July	Influent	1.08	1.12	189.93	220.10
	Effluent	1.25	1.15	58.42	91.08
13-August	Influent	1.09	0.84	389.68	267.79
	Effluent	0.86	0.83	82.67	133.49
14-August	Influent	0.80	0.85	353.70	201.76
	Effluent	0.91	0.90	88.94	83.76
21-August	Influent	0.61	0.75	385.93	267.03
	Effluent	0.91	0.94	66.43	120.79
1-August	Influent	1.05	1.12	337.71	252.97
	Effluent	1.30	0.93	22.04	36.77
7-August	Influent	0.79	1.06	384.97	182.18
	Effluent	1.35	1.14	4.11	5.55
23-August	Influent	0.78	0.87	365.21	244.67
	Effluent	0.83	0.55	25.44	5.01
26-September	Influent	0.86	0.77	99.40	145.77
	Effluent	0.66	1.34	15.79	4.98

k Shape factor of gamma distribution function
λ Scale factor of gamma distribution function

Influent and effluent refer to untreated and treated rainfall-runoff, respectively. The line separating the first set of events and the second set of events represents the breakpoint between the BHS events (top) and the VCF events (bottom).

Table 2-6. Summary of event-based particle number density (PND) indices.

Event Date (2010)		PND (µm) d_{10}		d_{50}		d_{90}	
		Manual	Auto	Manual	Auto	Manual	Auto
31-July	Influent	1.4	1.5	2.0	2.1	4.3	4.3
	Effluent	1.4	0.9	2.0	1.4	4.1	3.1
13-August	Influent	0.5	0.4	0.9	0.8	1.9	1.8
	Effluent	0.4	0.4	0.5	0.5	1.1	1.1
14-August	Influent	0.8	0.5	1.2	0.8	2.6	1.9
	Effluent	0.4	0.4	0.5	0.5	1.1	1.1
21-August	Influent	0.4	0.4	0.5	0.6	1.2	1.3
	Effluent	0.3	0.3	0.5	0.5	1.0	1.0
1-August	Influent	1.0	1.1	1.8	1.8	3.6	3.6
	Effluent	1.0	1.0	1.2	1.2	2.5	2.4
7-August	Influent	0.5	0.5	0.9	0.9	2.1	1.7
	Effluent	0.3	0.3	0.5	0.5	1.0	1.0
23-August	Influent	0.5	0.4	0.9	0.7	2.0	1.6
	Effluent	0.8	0.9	1.3	1.5	2.2	2.5
26-September	Influent	0.4	0.3	0.6	0.5	1.3	1.1
	Effluent	0.5	0.4	0.9	0.7	1.5	1.5

Influent and effluent refer to untreated and treated rainfall-runoff, respectively. The line separating the first set of events and the second set of events represents the breakpoint between the BHS events (top) and the VCF events (bottom).

Table 2-7. Summary of event-based power law model parameters for PND.

Event Date (2010)		α		β	
		Manual	Auto	Manual	Auto
31-July	Influent	4.44×10^{7}	5.40×10^{7}	2.03	2.09
	Effluent	6.89×10^{7}	4.79×10^{7}	2.38	2.12
13-August	Influent	2.25×10^{8}	1.53×10^{7}	2.40	2.13
	Effluent	4.61×10^{7}	5.79×10^{7}	2.37	2.37
14-August	Influent	6.53×10^{7}	4.37×10^{7}	2.09	2.31
	Effluent	4.97×10^{7}	3.33×10^{7}	2.35	2.30
21-August	Influent	2.84×10^{7}	7.52×10^{7}	2.47	2.29
	Effluent	3.72×10^{7}	2.70×10^{7}	2.45	2.25
1-August	Influent	3.56×10^{6}	1.15×10^{8}	2.18	2.17
	Effluent	1.52×10^{8}	8.91×10^{7}	3.45	2.92
7-August	Influent	5.16×10^{7}	2.38×10^{8}	2.31	2.41
	Effluent	8.63×10^{8}	4.65×10^{8}	3.89	3.67
23-August	Influent	2.84×10^{8}	1.12×10^{8}	2.26	2.31
	Effluent	8.13×10^{7}	3.87×10^{8}	3.08	4.13
26-September	Influent	8.51×10^{7}	9.57×10^{7}	2.49	2.50
	Effluent	1.26×10^{8}	3.94×10^{8}	3.26	3.71

α coefficient of the power law model (PLM), physical index for number of particles
β exponent of PLM, physical index for slope on log-log plot and size distribution of PM

Influent and effluent refer to untreated and treated rainfall-runoff, respectively. The line separating the first set of events and the second set of events represents the breakpoint between the BHS events (top) and the VCF events (bottom). Both α and β are not statistically significantly different ($p > \alpha = 0.05$) between sampling methods for influent and for effluent.

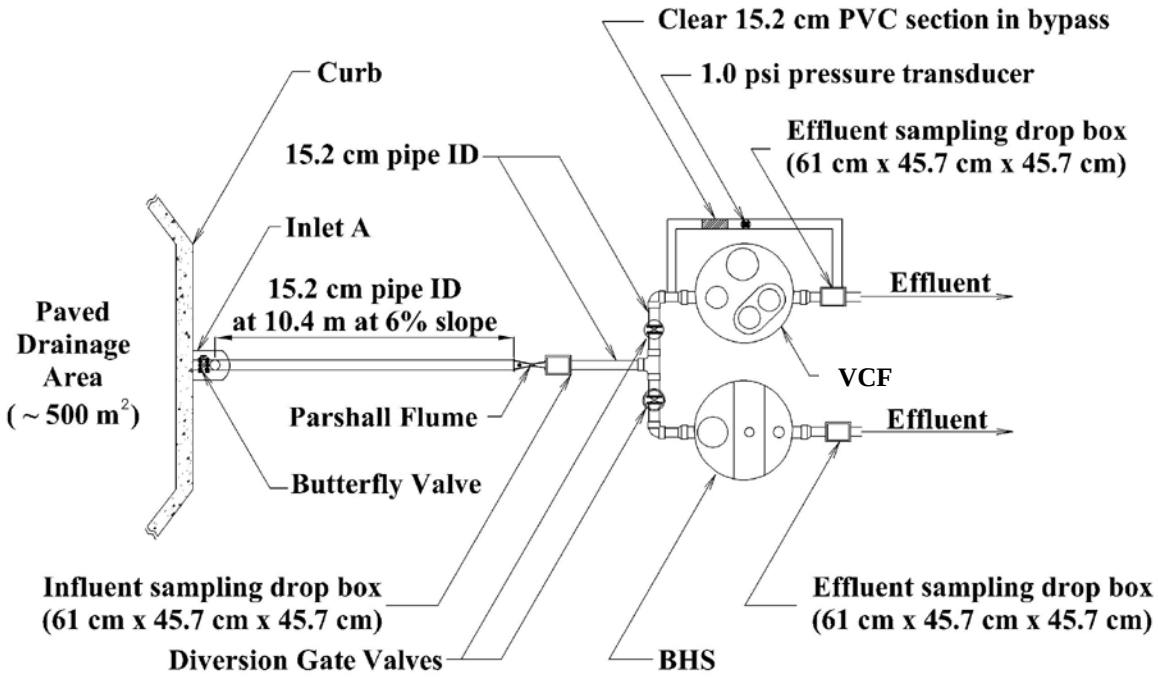

Figure 2-1. Elevation view of monitoring system design

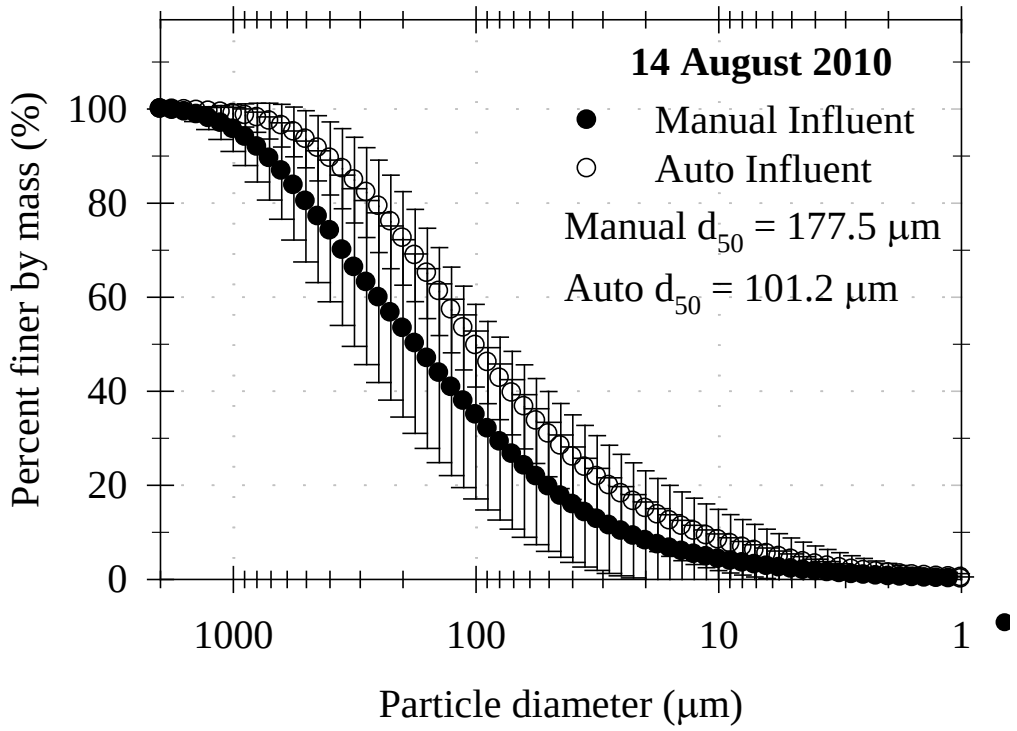

Figure 2-2. Example of manual and automated influent PSD (14 August 2010 rainfall-runoff event). Influent and effluent uncertainty bars represent the standard deviation in PSDs between all of the influent and effluent samples taken during a given event, respectively.

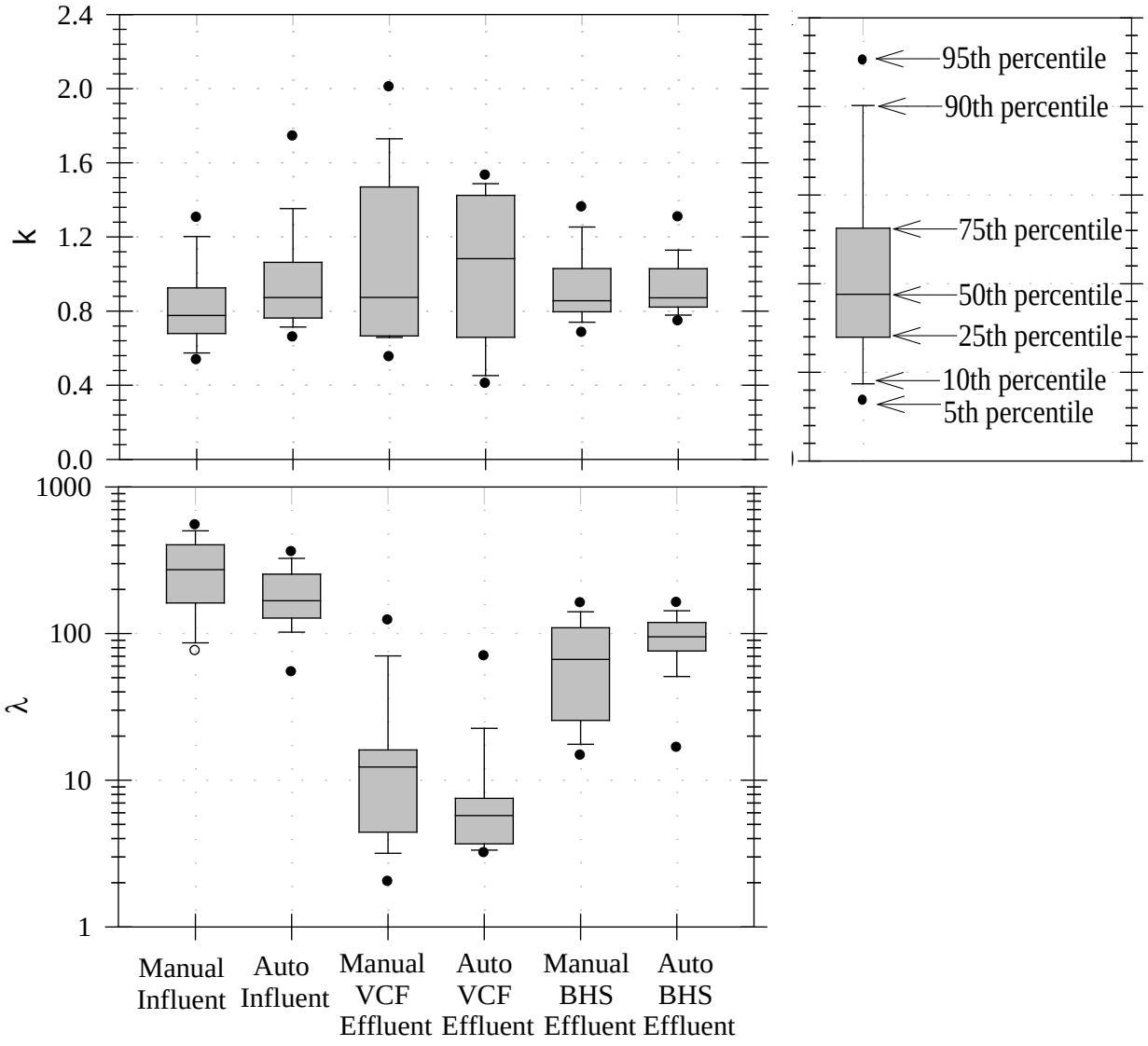

Figure 2-3. Manual and automated influent and effluent gamma distribution parameters

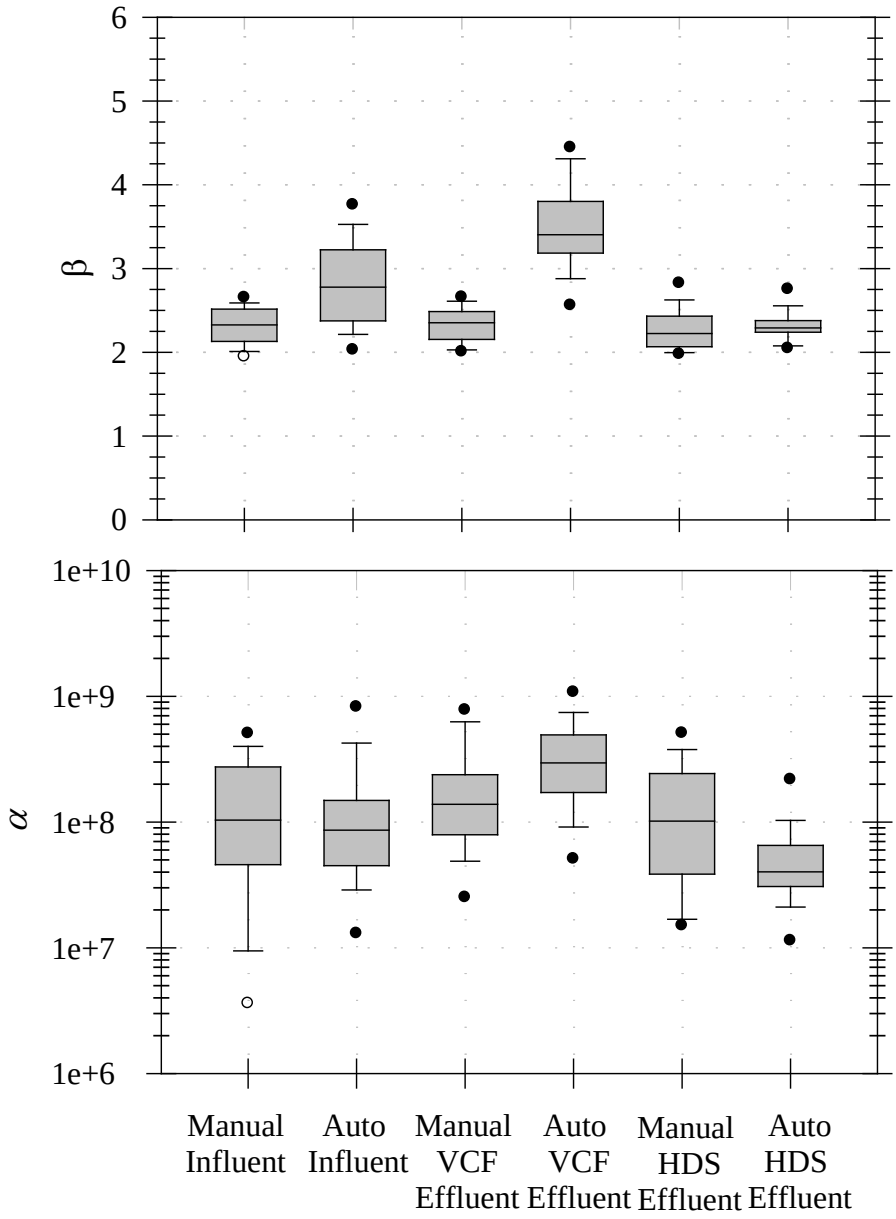

Figure 2-4. Manual and automated influent and effluent power law parameters for particles less than 75 µm

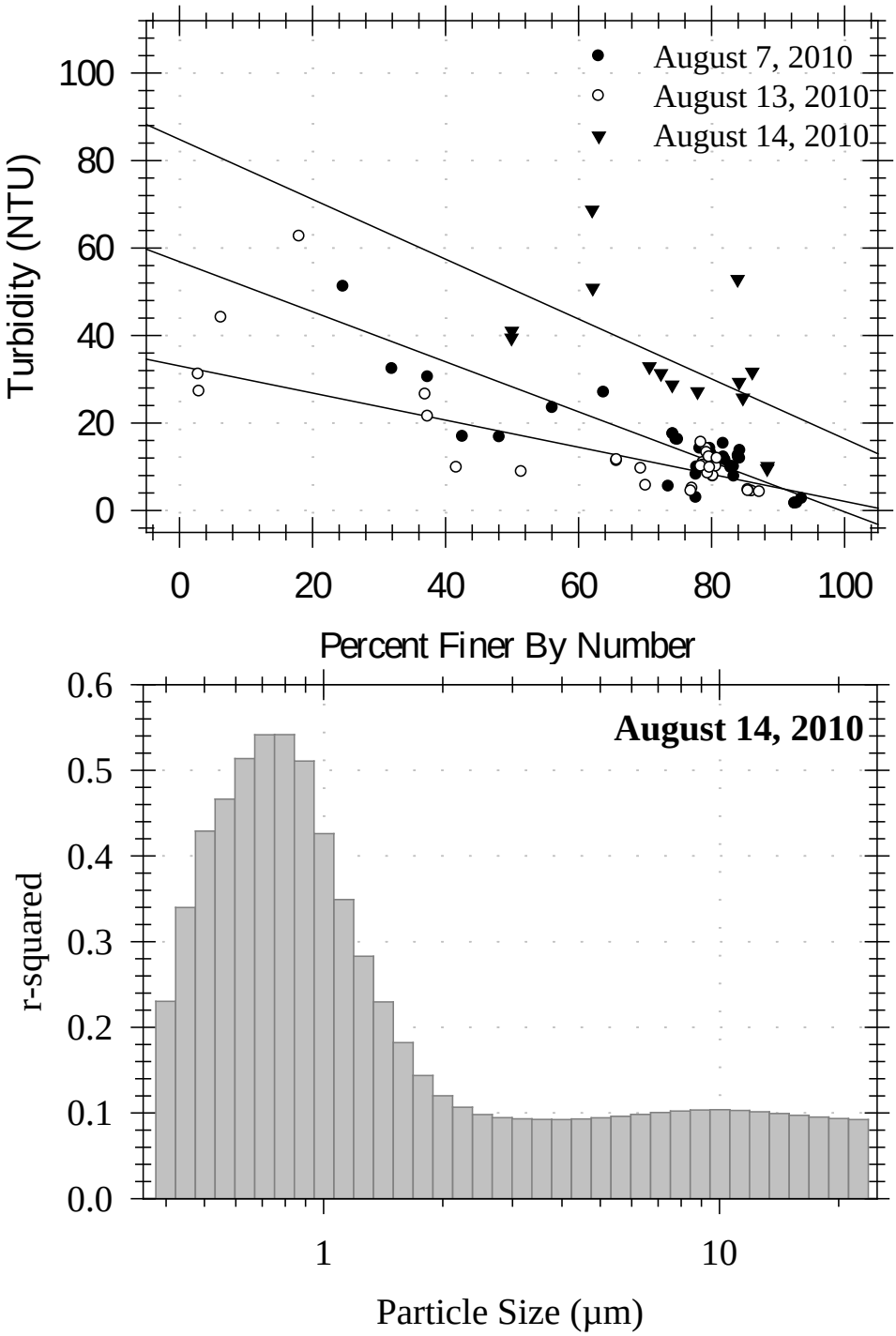

Figure 2-5. Relationship between turbidity and PND. The coefficient of determination between turbidity and percent finer by number is shown as a function of particle size (d = 0.02 – 25 µm).

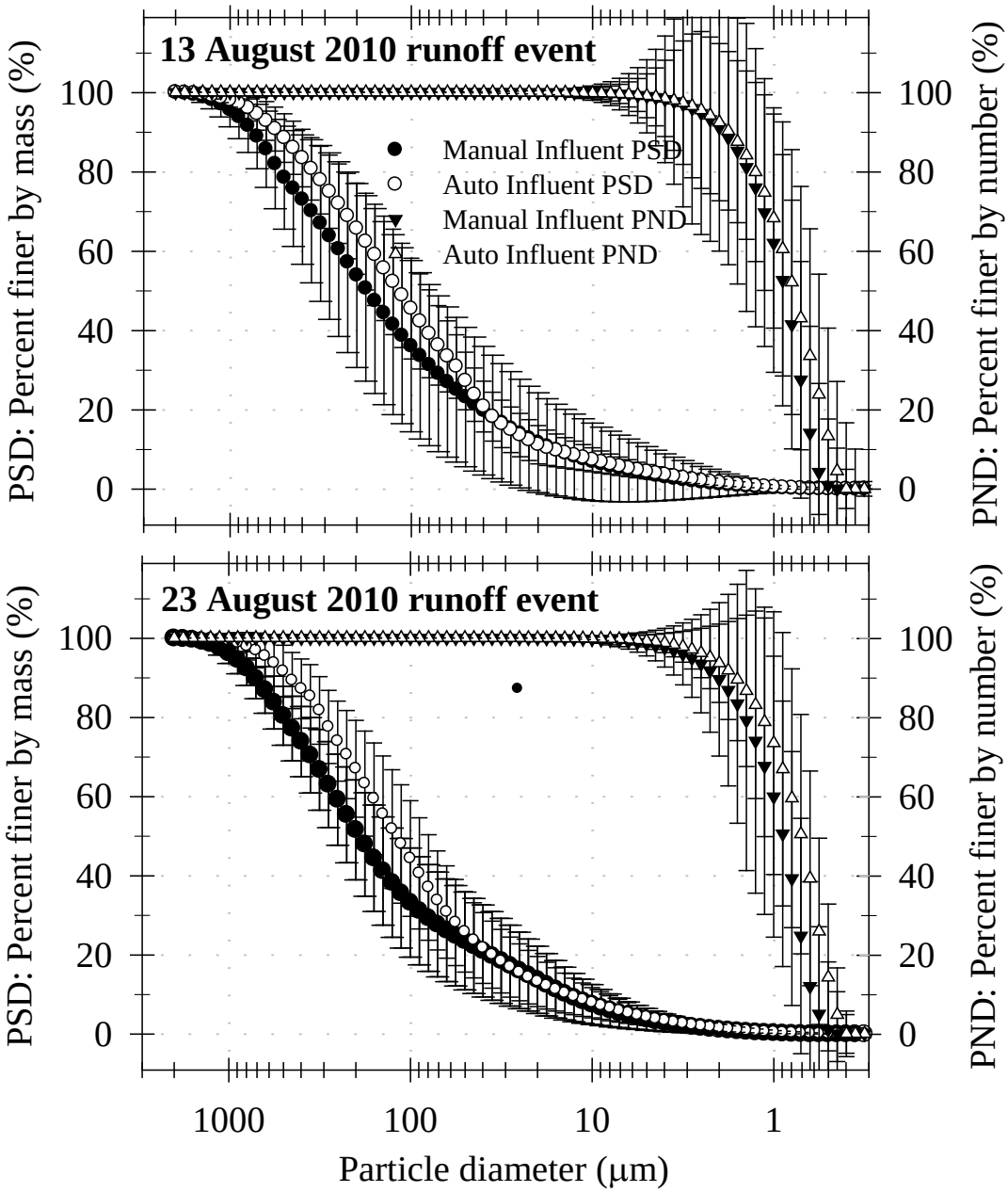

Figure 2-6. Examples of manual and automated influent PSD vs. PND (13 August 2010 and 23 August 2010 rainfall-runoff events). PSD method results are significantly different ($p \leq \alpha = 0.05$). PND method results are not significantly different ($p > \alpha = 0.05$).

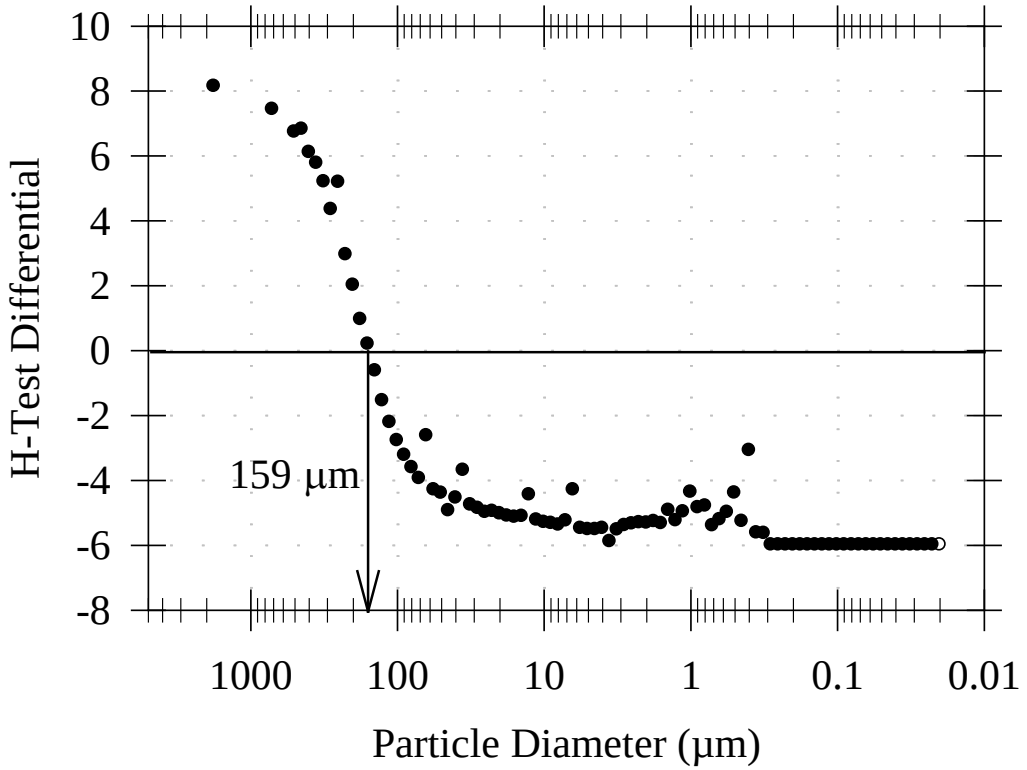

Figure 2-7. Kruskal-Wallis H test results for PSD. The difference between the critical H value and the measured H value increases with increasing particle size from 0.02 to 2000 µm. At a particle diameter of 159 µm the difference between the two values becomes so great that there is a statistically significant difference ($p \leq \alpha = 0.05$) between automated and manual samples. For all particle diameters greater than or equal to 159 µm, there is a significant difference between the two sampling techniques.

CHAPTER 3
PARTICULATE MATTER AND PHOSPHORUS REMOVAL IN RAINFALL-RUNOFF TREATED WITH VOLUMETRIC FILTRATION

Introduction

Rainfall-runoff from impervious surfaces and urban land use carries particulate matter (PM), nutrients (Marsalek, 1999; Vaze and Chiew, 2003), heavy metals (Liebens, 2001; Sansalone and Cristina, 2004; Lau and Stenstrom, 2005), and other constituents (Van Dolah et al., 2005; Khan et al., 2006) to lakes, streams, and rivers. Studies have identified non-point-source (NPS) pollution from urban rainfall-runoff as the leading cause of impairment across all types of waterbodies (EPA, 2000; Lee and Bang, 2000; Gnecco et al., 2005). This is partly due to the ecological impacts of particles on receiving waters and partly because many constituents of concern, including metals and nutrients, partition into the PM and are transported to surface waters in urban rainfall-runoff (Legret and Pagotto, 1999; Sansalone and Kim, 2008; Liu et al., 2010). An excessive concentration of phosphorus is believed to be the leading cause of eutrophication in freshwaters (Corell, 1998). In order to reduce the adverse effects of rainfall-runoff on surface waters, the water resources community has been forced to undertake the challenging task of monitoring stormwater quality (Harmel et al., 2003).

The Role of Urban Development

The PM found in rainfall-runoff originates from many sources in the urban environment (Sansalone and Kim, 2008). Infrastructure such as roads, sidewalks, and residential structures that are added during land development and urbanization significantly increase the runoff volumes and mass loads discharged to receiving waters (Glen et al., 2004; Gobel et al. 2007). Urban development decreases the amount of permeable surface in a watershed (Roesner, 1999). Additionally, with urbanization comes increased population density leading to contributions of dirt, contaminants from vehicles, debris from streets, and publicly used chemicals to urban

rainfall-runoff from these impervious surfaces (Sartor and Boyd, 1972; Grottker, 1987; Pratt et al., 1995). Activities such as transportation and urban infrastructure maintenance generate significant PM ranging in size anywhere from less than 1 μm to greater than 10,000 μm (Sansalone and Kim, 2008). A study by Sartor and Boyd showed that concentrations of suspended solids, nutrients, and other constituents are much higher in urban rainfall-runoff than in runoff from rural areas (1972). This impact greatly depends on traffic density, wind drift, duration and intensity of rainfall events, and duration of dry weather periods between events (Gabel et al., 2007).

History of Stormwater Regulations

Stormwater runoff (rainfall-runoff and snowmelt) was first recognized as a potential source of surface water impairment in the 1960s when government agencies first began to research the issue. At this time it was determined that stormwater runoff was responsible for almost half of all pollutant load discharged to surface waters (Pitt et al., 1999).

In response to growing concern, the Clean Water Act (CWA) was amended in 1987 to prohibit the discharge of pollutants from stormwater runoff to receiving waters unless it was in compliance with a National Pollutant Discharge Elimination System (NPDES) permit. This included industrial and construction stormwater discharges along with municipal separate storm sewer systems (MS4s).

In 1990, federal regulations (Phase I) were enacted to guide municipalities in preparing NPDES permit applications. In order to comply, municipalities had to collect existing information about the quantity and quality of stormwater discharge, receiving waters, management programs, and financial resources. Then, they had to create a program to reduce NPS pollution to the maximum achievable extent. Phase I applied to all medium and large

MS4s, cities with populations greater than 100,000, operators of construction activities affecting at least 5 acres of land, and certain industrial activities (EPA, 2000).

In 1999, the final rule (Phase II) was published by the Environmental Protection Agency (EPA). None of the permit requirements changed in Phase II, but they now additionally applied to all small MS4s located within an urban area with a population of at least 50,000 and a population density of at least 1,000 people per square mile along with operators of construction activities affecting at least 1 acre of land. Phase II permit coverage became mandatory in 2003 (EPA, 2000).

Current Research

In response to the NPDES amendments of the CWA, unit operations are being explored for the separation of PM in stormwater treatment (Nix et al., 1988; James, 1999). In many urban areas where there is limited area and high land cost, combined unit operations are preferred to extended treatment processes and large settling basins (Grizzard et al., 1986). Preliminary unit operations such as hydrodynamic separators were initially favored for their small footprint (Wong et al., 1995; Walker et al., 1999). However, since hydrodynamic separators primarily remove gross solids and require frequent maintenance, over the last decade filtration unit operations have become more common for PM separation in runoff (Liu et al., 2010). Such filtration unit operations can be implemented in a variety of configurations, including replaceable radial cartridge filters (Pathapati and Sansalone, 2009) and axial filters. The selection and design of filtration unit operations depends on knowledge of PM load and granulometry (Greb and Bannerman, 1997; Cristina et al., 2002; Sansalone and Kim, 2008), unit filter run volume, head-loss development, and desired effluent water indices such as suspended sediment concentration (SSC), total suspended solids (TSS), turbidity, and particle size distribution (PSD) (Clark, 2000). It is therefore critical, when assessing the performance of a stormwater treatment unit, to

quantify and qualify the inputs to the unit and the outputs to receiving waters under a variety of event durations, flow intensities, and loads (Liu et al., 2010).

Objectives

The primary objective of this study is to evaluate the removal of particulate matter using an in-situ volumetric clarifying filter (VCF) treatment unit. Variable flow rates, storm durations, and pollutant loads are tested and subsequent event mean values (EMVs) are calculated in order to evaluate the performance of a VCF during actual rainfall-runoff events. Performance, in terms of total mass load reduction and effluent particle size distribution, is evaluated for each of the two main mechanisms of removal in the unit, sedimentation and filtration. An additional objective of this study is to evaluate the removal of dissolved and particulate-bound phosphorus using the same treatment device.

Methodology

Watershed Configuration

The Reitz Union paved surface parking facility located on the University of Florida campus serves as the watershed in this study. Rainfall-runoff is collected from an existing stormdrain inlet at the southwest parking lot pavement edge. The watershed is divided into two main sub-catchments, a parking area on the southeast side and an access road on the northwest side. Due to the parking lot's low slope in the direction of drainage, the contributing watershed area varies with rainfall intensity and wind direction. Depending on the storm event, the watershed area varies from 400 to 600 square meters with a median area of approximately 500 square meters.

Volumetric Clarifying Filter and Monitoring System

This study utilizes a volumetric clarifying filter (VCF) for runoff treatment as shown in Figure 3-1. The VCF unit is 1.2 meters in diameter and is configured with two standard

cartridges, each with a 70-millimeter-orifice cartridge lid, and one draindown cartridge with a 35-millimeter-orifice cartridge lid. Each cartridge contains eleven 20-micrometer filter tentacles made up of two 69-centimeter long segments. The system components include a 46 centimeter diameter maintenance access pipe, a pressure relief pipe, a cartridge deck, a backwash pool weir located around the two standard cartridges, a separator skirt, and a settling zone. The unit has a maximum treatment flow rate (MTFR) of 12.6 liters per second and is configured to begin bypassing flow when head loss reaches 46 centimeters. This is equivalent to a water elevation of 46 centimeters above the cartridge deck level.

The monitoring station design is driven by the monitoring procedures related to the physical-chemical processes being investigated; PM and phosphorus removal. Rainfall-runoff chemistry is monitored across the treatment system during rainfall events. Runoff is transported to the treatment system after collection by catch basin Inlet A as shown in Figure 2-1. The cylindrical manhole is characterized by a 9-inch high inlet at the top and a 6-inch diameter outlet pipe at the bottom. A butterfly valve is used at the inlet to prevent unwanted flow from entering the system. A 15-centimeter diameter PVC pipe carries runoff at a 6 percent slope from the inlet to a Parshall flume located 10 meters downstream. A 61 cm x 46 cm x 46 cm influent sampling drop box is located immediately downstream of the Parshall flume. A 15-centimeter diameter PVC tee-section carries the runoff from the outfall of the drop box to the treatment unit. Diversion gate valves are used on each side of the tee to direct all of the influent runoff either to the VCF or to a BHS that is installed in parallel for a separate study. A 61 cm x 46 cm x 46 cm effluent sampling drop box is located at the outfall.

Additionally there is a bypass pipe network for the VCF. It consists of a 15-centimeter diameter PVC pipe elevated to 122 centimeters above the unit's internal cartridge deck level,

with a 5-centimeter diameter siphon break 30 centimeters above that. In the event that bypass occurs during an event treated by the VCF, untreated bypass effluent and treated effluent are sampled either as a composite or as two individual streams in the effluent sampling drop box. None of the events monitored for this study generated bypass.

In order to investigate the head loss caused by the 20-micrometer filter tentacles during rainfall-runoff events, continuous head measurements are taken both inside and outside of the filter cartridges. Two 1-psi pressure transducers (model PDCR-1830 1 psig) are used for these measurements (DRUCK Inc.). Measured differences in water depth from the two sensors provided the head loss caused by the filters. Additionally, bypass flow rate is measured with a 1-psi pressure transducer located in the bypass pipe (model PDCR-1830 1 psig). The CR1000 model data logger manufactured by Campbell Scientific Inc. is used for the transducers.

In order to measure flow depth, the Parshall flume is equipped with a Shuttle Level Transmitter model ultrasonic sensor which is calibrated at the site to measure water depth. An MJK 4-20mA model data logger is used for the sensor.

The site is equipped with a tipping bucket rain gauge manufactured by ISCO Inc. (0.01 inch bucket capacity). It is located on the roof of the Stormwater Unit Operations and Processes (UOP) laboratory, which is about 180 meters southwest of the watershed. Additionally, two rain gauges located at the University of Florida's Physics Department (west side of catchment) and at the University of Florida's Dental Tower (south-east side of catchment) provide a validation of rainfall measurements.

The roof of the UOP laboratory has also been equipped for rainfall chemistry monitoring. In addition to the manually sampled rainfall-runoff, rainfall is collected on the roof prior to

reaching the ground. Four DI rinsed Pyrex dishes are used for rainfall collection during the events.

Calibration Procedures

Calibration of MJK ultrasonic sensor for flow depth measurements

A Shuttle Ultrasonic sensor manufactured by MJK is mounted 76 cm above the invert surface of the Parshall flume. The sensor has an accuracy of $\pm$ 0.10 cm. The sensor is connected to a logic unit equipped with a display that converts the voltage response to water depth once the sensor has been properly installed and leveled and the system has been calibrated. The initial setup consisted of selecting the output unit (inches) and adjusting the zero level to an absolute reference value. For this the invert surface of the flume is cleaned and dried and a sensor measurement is taken. This value is then set as the "control" reading. Then a series of discrete depths are generated for the expected range of flow depths. Measurements are recorded and a calibration curve is developed.

Calibration of pressure transducers

The three 1-psi pressure transducers (DRUCK Inc.) are connected to the CR1000 data logger (Campbell Scientific Inc.). During the calibration phase the real time data are acquired and monitored by a field laptop connected to the data logger. Pressure data are reported as mV and converted to water depth (feet) through a calibration curve unique to each pressure transducer. The calibration phase consisted of placing each transducer in a water column under static conditions. Various water depths are measured manually and the corresponding voltage measurements are recorded. A linear regression between voltage measures and water depth provided the multiplier and offset parameters. These parameters are then input into the sensor's data acquisition program.

Preliminary hydraulic testing

Hydraulic testing is performed to quantify the clean-bed (time 0) head loss as a function of steady flow across the VCF. Clean-bed, potable water (TSS < 0.1 mg/L) head loss measurements are taken by two, 1-psi pressure transducers at steady increments of flow rates. The VCF's internal deck is used as the datum for all head measurements. During the testing, the VCF is configured to have two standard cartridges with 70 mm orifice lids and one draindown cartridge with a 35 mm orifice lid. This is the same configuration that is used for actual rainfall-runoff events. Water is pumped through the system at 20-gpm increments starting at 40 gpm, peaking at 260 gpm, and returning to 40 gpm. Flow rate is regulated with a flow meter.

Monitoring Methodology

A threshold rainfall depth of 2.5 mm and a minimum dry period of 6 hours are selected for rainfall-runoff events. Prior to an event, radar tools such as Wunderground (www.wunderground.com) and National Weather Service (NWS) are utilized to determine if an approaching rainfall event is of sufficient intensity, spatial coverage, and trajectory. Although the monitoring station is permanently assembled, some setup prior to an event is required. The YSI Multi Parameter sensor, the MJK Ultrasonic level sensor, and the pressure transducers are connected to the CR1000 data logger. Two synchronized stop watches are used for sampling, one each for influent and effluent.

Runoff samples are taken manually at two sampling points, one upstream of the treatment system and one downstream of the treatment system, at regular intervals in the range of two to five minutes. Frequency is determined based on radar and rainfall intensity/flow inspections. Manual samples are taken across the full cross-section of flow, with mathematical compositing based on measured flow volume and time.

For both influent and effluent sampling, one set of 1.1-L replicate samples and two sets of 0.5-L replicate samples are taken. One of the sets of 0.5 L samples is used for a particle size distribution (PSD) analysis. The other set is used to determine SSC. Corresponding PSD and SSC results are paired so that the PSD results (volume %) are converted to a gravimetric concentration (mg/L). The set of 1.1 L samples is used to determine turbidity, sediment PM, settleable PM, TSS, and dissolved and particulate-bound phosphorus.

Assessing PM Loads and Transport in Urban Rainfall-Runoff

At the end of a monitored event, samples are taken back to the laboratory for analysis. The rainfall is also collected from the Pyrex troughs for immediate analysis. The first analysis in the lab uses laser diffraction on a set of 0.5 L samples to determine PSD. This is done for runoff samples only. The laser diffraction particle analyzer (Malvern Instruments: Hydro 2000G) is operated in batch mode. Prior to being poured into the analyzer, each sample is prescreened with a #4 2000-µm sieve. This is done so that PM or other debris larger than 2000 µm is not allowed to enter the laser chamber. Once samples are added to the wet chamber of the analyzer, multiple repetitions (3-9) are required until the entire gradation reaches stability.

A paired SSC analysis is conducted within the first 24 hours following an event. This is done for runoff samples only. For the SSC analysis, the other set of 0.5-L samples is filtered through a 1-µm glass fiber filter using a vacuum pump. Filters are washed, dried, and weighed prior to use. The sample volumes are recorded and filters are dried in an oven at 105ºC. Final filter weights are then recorded. The difference between final and initial filter weights provides the mass of PM, which can then be converted to a concentration (as SSC) with sample volume.

The set of 1.1-L samples is analyzed in parallel with the PSD and SSC analyses. These samples are first used for turbidity measurements. Then, samples are screened through a #200 75-µm sieve in order to separate and collect sediment-size particles. The sample volume is

measured and recorded prior to sieving. The filtrate is then poured into an Imhoff cone and allowed to settle for one hour under quiescent conditions. At the end of the hour, the settleable PM is carefully recovered from the Imhoff cone by decanting the supernatant from the cone and collecting the PM from the bottom. The settleable PM is placed in a pre-weighed pan, dried at 105ºC, and a final weight is recorded.

A volumetric fraction of the Imhoff cone supernatant (60 mL) is then passed through a pressurized stainless-steel fractionation column with a 0.45-µm membrane using a vacuum pump. The fractionated filtrate is used immediately for total dissolved phosphorus (TDP), measured with a HACH DR 5600 Spectrophotometer. The 0.45-µm filters used for fractionation are preserved at 4ºC for total suspended phosphorus analysis.

The remainder of the Imhoff cone supernatant is used to determine the suspended PM fraction (as TSS). About 100 mL is taken from the well-mixed supernatant and filtered through a 1-µm glass fiber filter using a vacuum pump. Filters are washed, dried, and weighed prior to use. The sample volumes are recorded and filters are dried in an oven at 105ºC. Final filter weights are then recorded. The difference between final and initial filter weights provides the mass of PM, which can then be converted to a concentration (as TSS) with sample volume.

The following fractions of phosphorus are measured by the spectrophotometer (HACH DR 5600): TDP, sediment-bound total phosphorus, settleable-bound total phosphorus, and suspended-bound total phosphorus. The method used for the measurement of phosphate (soluble reactive phosphorous) (orthophosphate) is Standard Method 4500-P-E Ascorbic Acid method. A HACH DR 5600 spectrophotometer is used to determine phosphate concentration. To determine sediment-bound and settleable-bound total phosphorus, small amounts (0.5 g) of sediment-PM and settleable-PM are acid-digested. To determine suspended-bound total phosphorus, the 0.45-

μm membranes from the fractionation process are acid-digested. To determine the TDP, fractionated filtrate is analyzed in the spectrophotometer.

As part of the quality assurance/quality control (QA/QC) procedure, all probes are calibrated with known standards. For the ions analyzed by the spectrophotometer, calibration curves for reagents are developed with at least 5 data points. The coefficient of determination R^2 must be greater than or equal to 0.99. A new 5-point calibration curve is created for each new reagent lot number.

Data Analysis and Elaboration

Volumetric rainfall-runoff coefficients

The runoff coefficient in this study is a volumetric-based coefficient ranging from 0 to 1. It represents the fraction of runoff resulting from a known volume of rainfall across an entire event. The volumetric runoff coefficient is expressed as equation 3-1.

$$c = \sum_{n} \frac{Q_n}{I_n \times A_w} \tag{3-1}$$

In this expression, c represents the runoff coefficient, Q_n represents the volumetric flow rate of sample period n observed at the outlet (L^3/s), I_n represents the rainfall intensity of the nth interval (L/s), and A_w represents the median contributing area of the watershed (L^2).

Event mean value

While the inter-event distributions of PM and phosphorus are log-normal, a volume-weighted event mean value (EMV) is utilized as a comparative index for characterizing PM and phosphorus concentrations that represent a flow-weighted PM and phosphorus concentration for a rainfall-runoff event (Sansalone and Kim, 2008). EMV is calculated using equation 3-2.

$$EMV = \frac{\sum_{i=1}^{n} C_i V_i}{\sum_{i=1}^{n} V_i} = \overline{C} \qquad (3\text{-}2)$$

In this expression, C_i represents the average value associated with period i (often mg/L), V_i represents the volume of flow during period i (L), and $\overline{C}$ represents the flow-weighted average value for an entire event (often mg/L).

Removal efficiency

Treatment capacity is often quantified as a percent removal. This is calculated for the constituent of interest using the inflow and outflow loads and equation 3-3.

$$PR(\%) = \frac{\sum_{i=1}^{n} (V_{i-IN} \times C_{i-IN}) - \sum_{j=1}^{m} (V_{j-EFF} \times C_{j-EFF})}{\sum_{i=1}^{n} (V_{i-IN} \times C_{i-IN})} \times 100 \qquad (3\text{-}3)$$

In this expression, $V_{i\text{-}IN}$ is the volume of influent flow for sampling period i (L); $V_{j\text{-}EFF}$ is the volume of effluent flow for sampling period j (L); $C_{i\text{-}IN}$ is the mean influent concentration associated with period i (mg/L); $C_{j\text{-}EFF}$ is the mean effluent concentration associated with period j (mg/L); n is the total number of influent measurements taken during an event; m is the total number of effluent measurements taken during an event.

Particle size distribution (PSD)

PSD is useful in characterizing PM. The output of the laser diffraction instrument is in percent finer by volume. A more useful unit is percent finer by mass, which can be used to find a d_{10}, a d_{50}, and a d_{90}. In order to make this conversion, the measured gravimetric mass (from SSC) is distributed over the entire PSD for each sample. Mass-based cumulative PSDs (i.e. percent finer by mass) for the samples are computed by integrating the gravimetric concentration

of individual particle sizes for samples, corresponding flow rates, and sampling time intervals. With this paired data, PM total volume concentration for each particle size is converted to a gravimetric concentration in mg/L.

Mass balance error

A mass balance is often conducted after all of the events are captured in order to ensure mass conservation based on influent mass, effluent mass, and recovered PM mass trapped in the treatment unit due to sedimentation and filtration. A mass balance error (MBE) of 10% is chosen as the maximum allowable for this study. MBE is calculated using equation 3-4.

$$MBE(\%) = \frac{\left[\sum M_{\text{inf}} - \left(\sum M_{eff} + \sum M_{rec}\right)\right]}{\sum M_{\text{inf}}} \times 100 \qquad (3\text{-}4)$$

In this equation, ΣM_{inf} and ΣM_{eff} are the cumulative mass load of influent and effluent across the entire event, respectively, ΣM_{rec} is the total mass of PM recovered after an event, including PM trapped by sedimentation and filtration.

Mann-Whitney U test for significant difference

When comparing two sets of data, a useful test for significant difference in data that is not normally distributed is the Mann-Whitney U test. For this test, a U value is calculated for each set of data, or treatment, and the lowest U is compared to a critical U value from a U table. U values are calculated by combining all the samples in the k treatments and ordering them from smallest to largest. Each sample is assigned a rank, with the smallest sample value being assigned first rank and the largest sample value being assigned nth rank. If any 2 or more data points are equal, each is assigned the average of the ranks. Next, the samples are divided into their original treatment groups and the ranks for each treatment are summed. A U value for each treatment is then calculated using equation 3-5.

$$U_i = r_i - \frac{s_i(s_i + 1)}{2} \quad (3\text{-}5)$$

In this expression, r_i is the rank sum for treatment i, s_i is the number of samples in treatment i. When the smallest of the calculated U values exceeds the critical U value, the conclusion is that the two treatment means are significantly different.

Newton's law

Settling velocity of a spherical particle in a fluid is calculated using Newton's Law provided in equation 3-6.

$$V_s = \sqrt{\frac{4g}{3C_d} \times \frac{\rho_p - \rho_f}{\rho_f} \times d_p} \quad (3\text{-}6)$$

In this expression, V_s is the settling velocity, g is the gravitational acceleration, ρ_p is the particle density, ρ_f is the fluid density, C_d is the frictional drag coefficient, and d_p is the particle diameter. C_d is calculated using equation 3-7.

$$C_d = \frac{24}{R_d} + \frac{3}{\sqrt{R_d}} + 0.44 \quad (3\text{-}7)$$

In this expression, R_d is the particle Reynolds number, which can be calculated for the transitional settling region using equation 3-8.

$$R_d = \frac{\rho_f d_p V_s}{\mu_f} \quad (3\text{-}8)$$

In this expression, ρ_f is again the fluid density, d_p is again the particle diameter, V_s is again the settling velocity, and μ_f is the fluid viscosity.

Surface overflow rate

The critical settling velocity is equal to the surface overflow rate which is calculated using equation 3-9.

$$SOR = V_{s,crit} = Q/A_s \quad (3\text{-}9)$$

In this expression, SOR is surface loading rate, $V_{s,crit}$ is the critical settling velocity, Q is the flow rate, and A_s is the surface area.

Surface loading rate

The surface loading rate is calculated using equation 10.

$$SLR = Q/A_{filter,s} \quad (3\text{-}10)$$

In this expression, SLR is surface loading rate, Q is the volumetric flow rate, and $A_{filter,\ s}$ is the entire surface area of the filter.

Cumulative gamma distribution (CGD) function

The PSDs are modeled gravimetrically using a cumulative gamma distribution (CGD). In order to represent any PSD both a dispersivity parameter and a representative parameter of PM size for the PSD are needed. The dispersivity parameter can be thought of as a characteristic of gradation uniformity or for example as a PM size sorting coefficient (Dickenson and Sansalone, 2009). Therefore a series of PSDs with the same representative PM size parameter but differing shapes can be generated. The PM size parameter is a representation of the fineness or coarseness of a PSD, for example a phi-scale (ϕ_n) particle size gradation parameter or more commonly a d_{50m}, where "m" indicates on a gravimetric basis (Dickenson and Sansalone, 2009). To model PSDs of differing uniformity and PM size representation is required for influent and effluent urban runoff. Previous studies (Sansalone and Ying, 2008; Lin et al., 2009) have utilized a two parameter CGD to model size heterodisperse PSDs. The shape and scale factor parameters in the CGD, k and λ, are physically analogous to the uniformity of the PSD and the representative

coarseness or fineness of the PSD. Equations 3-11 and 3-12 represent the gamma distribution (*f(x)*) and CGD (*F(x)*), respectively.

$$f(x) = \frac{(x/\lambda)^{k-1} e^{(-x/\lambda)}}{\lambda \times \Gamma(k)} \quad (3\text{-}11)$$

$$F(x) = \int_0^x f(x)dx \quad (3\text{-}12)$$

In this expression x represents the particle diameter, d (μm), k represents a shape parameter, λ represents a scaling parameter and Γ(λ) is a gamma function.

Results and Discussion

Event Hydrology

Event-based hydrologic indices including previous dry hours (PDH), event duration (d_{rain}), peak flow rate (Q_{max}), median flow rate (Q_{med}), mean flow rate (Q_{mean}), total influent volume (V_i), total effluent volume (V_e), rainfall depth (h_{rain}), initial pavement residence time (IPRT), and runoff coefficient (c) for a total of 25 events occurring between May 28, 2010 and June 27, 2011 are shown in Table 3-1. For the 25 storms monitored in this study, event duration ranges from 26 to 691 minutes. IPRT ranges from 3 to 33 minutes. Runoff volume ranges from 205 to 13,229 liters. Peak rainfall intensity ranges from 5.1 to 137.2 mm/hr. Peak runoff flow rate ranges from 0.5 to 14.3 L/s, median flow rate ranges from 0.1 to 5.5 L/s, and mean flow rate ranges from 0.1 to 5.5 L/s. Rainfall depth ranges from 0.3 to 5.0 cm. Figure 3-2 illustrates the cumulative frequency distribution of event rainfall depth for Gainesville, FL based on historical data (NWS). The storms monitored in this study and their respective rainfall depths are also shown.

For the 25 storms monitored in this study, PDH range from 10 to 438 hours with a median of 75 hours. This median is for an entire year of study covering both the wet season and the dry

season. This result is consistent with previous years in Gainesville, Florida. Based on historical data from the last ten years (NWS), the overall average dry period between rainfall events is 82 hours. The dry period between rainfall events varies greatly with seasonality. For this study, the median dry period during the wet season and during the dry season is 66 hours and 164 hours, respectively. Based on historical data for Gainesville over the past ten years, the average dry period during the wet season and during the dry season is 69 hours and 96 hours. These results indicate that while the wet season monitored in this study is typical of Gainesville, the dry season is uncharacteristically dry.

The runoff coefficient for the site ranges from 0.12 to 0.83. The lowest runoff coefficient (0.12) is observed on the 20 April 2011 event characterized by low rainfall depth and intensity and the lowest runoff volume. The highest runoff coefficient (0.83) is observed on the 30 June 2010 event characterized by high rainfall intensity and a large runoff volume. These results for runoff coefficient are typical of urban catchments. A study by Cristina and Sansalone found similar results for a small urban catchment in Cincinnati, Ohio with ranges of 0.2 to 0.4 and 0.6 to 0.8 for low and high intensity events, respectively (2003).

Particulate Matter (PM)

PM-based studies are difficult to compare due to differences in methodologies. For example, sampling can be done manually or with automated samplers. However, this study has concluded that automated samplers are not designed to sample coarse size heterodisperse PM representatively, but instead are designed to sample size monodisperse suspended wastewater flocs. In addition to differences in sampling technique, the analyses performed affect the comparability of studies. TSS is often used in studies as a gravimetric index for PM. However, studies have shown that the required subsampling step of the TSS procedure can introduce errors due to the difficulty of taking a representative subsample. Furthermore, TSS only provides

information about fine particles (< 75 µm). Although coarse particles (> 75 µm) have been found to have lower pollutant concentrations (Sansalone and Buchberger, 1997; Roger et al., 1998; Lau and Stenstrom, 2005), they can be retained in treatment systems and result in clogging and a need for increased maintenance. An SSC analysis paired with PSD provides information about the entire gradation.

Event-based PM fractions including sediment PM, settleable PM, suspended PM, turbidity, SSC, and volatile suspended solids (VSS) for the 25 events are shown in Table 3-2. There is significant variability in the ratios of suspended, settleable, and suspended PM to total PM between the 25 events. PM fractions for both influent and effluent runoff are illustrated in Figure 3-3. The influent suspended fraction of PM ranges from 1 to 29% with a volume-weighted mean of 6%. The effluent suspended fraction of PM ranges from 17 to 69% with a volume-weighted mean of 54%. The influent settleable fraction of PM ranges from 0 to 30% with a volume-weighted mean of 9%. The effluent settleable fraction of PM ranges from 7 to 44% with a volume-weighted mean of 21%. The influent sediment fraction of PM ranges from 55 to 99% with a volume-weighted mean of 84%. The effluent sediment fraction of PM ranges from 12 to 65% with a volume-weighted mean of 24%. Figure 3-3 illustrates the dominance of the sediment PM fraction in the influent and the dominance of the suspended PM fraction in the effluent. This is due to the high removal of sediment and settleable PM fractions by the sedimentation and filtration processes utilized in the VCF unit. The percent removal of suspended PM ranges from 48 to 96% with a volume-weighted mean of 77%. The percent removal of settleable PM ranges from 65 to 99% with a volume-weighted mean of 92%. The percent removal of sediment PM ranges from 97 to 100% with a volume-weighted mean of

100%. The percent removal of total PM (as SSC) ranges from 89 to 100% with a volume-weighted mean of 98%.

Probability density functions (pdfs) for runoff flow rate, turbidity, suspended PM, settleable PM, sediment PM, and SSC are also developed for influent and effluent samples based on all 25 monitored events. The measured distributions are illustrated in Figure 3-4. All of the measured results for both influent and effluent samples are log-normally distributed with an R-squared greater than 0.90. Mann-Whitney rank sum tests are conducted on turbidity and PM fractions to compare influent results and effluent results. Results of the tests indicate that, for all PM fractions and for turbidity, the effluent is significantly lower ($p \leq \alpha = 0.05$) than the influent.

Particle Size Distribution (PSD)

The percentages finer by mass, d_{10}, d_{50}, and d_{90}, are shown in Table 3-3. The d_{50} represents the particle diameter for which 50 percent of the particles by mass are smaller than or the same size as that diameter. Similarly, the d_{10} and the d_{90} represent the particle diameters for which 10 and 90 percent of the particles by mass are smaller than or the same size as those diameters. For the 25 events monitored in this study, influent runoff d_{10} ranges from 2 to 54 µm with a median of 9 µm. Effluent runoff d_{10} ranges from 0 to 2 µm with a median of 1 µm. Influent runoff d_{50} ranges from 22 to 263 µm with a median of 82 µm. Effluent runoff d_{50} ranges from 1 to 11 µm with a median of 3 µm. Influent runoff d_{90} ranges from 173 to 1016 µm with a median of 401 µm. Effluent runoff d_{90} ranges from 2 to 52 µm with a median of 12 µm. The spread of the influent PSD range indicates that PM in the raw influent runoff is size heterodisperse and varies greatly with changes in rainfall intensity, traffic, and previous dry hours. This heterodispersity is illustrated in Figure 3-5 which shows the median PSD curve for the 25 monitored events influent runoff. The solid curve represents the median PSD, the upper and lower dotted curves represent the standard deviation of PSD across all events. The spread of the effluent PSD range is mainly

attributed to filter ripening. Filter ripening is the complex process by which a colmation layer, composed of protozoa, bacteria, and algae, develops on the filter and contributes to PM removal (Dizer et al., 2004).

PSD is highly dependent on hydrology. The most intense rainfall-runoff events occur on 21 June 2010, 1 August 2010, and 14 May 2011 with peak rainfall intensities of 121.9, 127.0, and 137.2 mm/hr, respectively. The 21 June event has the highest influent d_{10} and d_{50} values of 54 and 263 μm, respectively. The least intense events occur on 23 August, and 26 September 2010 and 20 April 2011 with peak rainfall intensities of 5.1, 5.1, and 15.2 mm/hr respectively. The 20 April event has the lowest d_{10} and d_{50} values of 2 and 22 μm, respectively. The 26 September event has the second lowest influent d_{10} and d_{50} values of 4 and 35 μm, respectively.

A comparison of PM removal and PSD between primary effluent (sedimentation only) and secondary effluent (sedimentation + filtration) is also conducted for the 25 storms. For this comparison, measured influent PM, PSD and flow data are used to model primary effluent PM and PSD for the VCF after sedimentation alone. For particles ranging from 0.02 to 2000 μm, settling velocity is calculated using Newton's law. Newton's law is widely used to model Type I (discrete) settling because it is applicable for all settling regions (laminar, transitional, and turbulent) (Metcalf and Eddy, 2003). An iterative computation of settling velocity is used with drag coefficient and Reynolds number. The flow rate at each sample time is used to calculate surface overflow rate, or the critical settling velocity at that sample time. Particle sizes with settling velocities greater than the critical settling velocity are assumed to be fully removed, whereas particle sizes with settling velocities less than the critical settling velocity are assumed to be removed at a fraction equal to the ratio of particle settling velocity to critical settling velocity (Lawson, 1994). For each particle size of a given sample, removal rates are applied to

the influent mass load and a new effluent SSC and PSD is generated from the result. The total mass load reduction during the sedimentation process ranges from 65 to 99% with a volume-weighted mean of 87% and effluent d_{50} ranges from 3 to 25 µm with a median of 10 µm. Mann-Whitney rank sum tests are conducted on primary and secondary effluent SSC results as well as primary and secondary effluent PSDs. Although both PM removal and effluent PSD of primary and secondary effluent are significantly different, the comparison indicates that PM is substantially removed by hydrodynamic separation alone. This is attributed to the large surface area of the treatment unit and the low median flow rate of rainfall-runoff during the 25 events monitored in this study, which generates relatively low surface overflow rates within the unit. Results of the PSD comparison are shown in Table 3-3 and results of the SSC comparison are shown in Table 3-4.

The most significant deviations between primary and secondary effluent occur during high flow events. The three events with the highest flow rates occur on 21 June, 30 June, and 1 August 2010 with median flow rates of 5.5, 3.3, and 4.7 L/s and average flow rates of 5.1, 4.0, and 5.5 L/s, respectively. These events have among the highest modeled event-based effluent d_{50} results of 21, 14, and 25 µm and the highest modeled event-based effluent d_{90} results of 44, 54, and 67 µm, respectively. The measured influent and effluent PSDs are shown with the modeled effluent PSD for the 1 August event in Figure 3-6.

Probability density functions (pdfs) for surface overflow rate (SOR) and surface loading rate (SLR) are developed from the 25 monitored events. The measured distributions are illustrated in Figure 3-7. Both SOR and SLR are log-normally distributed with an R-squared greater than 0.83. The distribution of SOR is indicative of the VCF unit's settling capacity as a function of influent flow rate. The median SOR across all events is 0.20 mm/s. This

corresponds to an equivalent particle diameter of 15 μm. The distribution of SLR is indicative of the typical load on the filters for a small watershed during rainfall-runoff events of varying intensity and duration. The median SLR across all events is 0.13 L/min/m^2. The maximum SLR during this study is 8.05 L/min/m^2, which is an order of magnitude below the optimum loading rate range for a typical granular filter (82 to 204 L/min/m^2) (Metcalf and Eddy, 2003).

Cumulative mass distributions of PM across the entire size gradation are modeled with a CGD. The modeling process fit parameters k and λ in the CGD function. The parameters are optimized by minimizing the sum of squared error (SSE) and maximizing the correlation coefficient, such that the p-value is greater than 0.05 between modeled and measured data. Cumulative trends are well behaved and consistently fit a CGD. For measured influent PSD, k ranges from 0.45 to 1.29 with a volume-weighted mean of 0.77 and λ ranges from 131 to 579 with a volume-weighted mean of 302. For modeled primary effluent PSD, k ranges from 0.79 to 2.00 with a volume-weighted mean of 1.28 and λ ranges from 2.0 to 27.5 with a volume-weighted mean of 14.3. For measured secondary effluent PSD, k ranges from 0.20 to 2.01 with a volume-weighted mean of 1.15 and λ ranges from 1.6 to 46.3 with a volume-weighted mean of 10.0. Event-based k and λ as a function of cumulative treated volume are illustrated in Figure 3-8. Gamma parameters for all events are shown in Table 3-5.

Phosphorus

Event-based phosphorus fractions including sediment P, settleable P, suspended P, dissolved P, and total P for the 25 events are shown in Table 3-6. Studies estimate that the EMV for total P resulting from urban rainfall-runoff is around 300 μg/L (Brown et al., 2003), considering both new and old urban development. The values found in this study are significantly higher. The volume-weighted influent total P of 3283 μg/L is an order of magnitude higher than concentrations reported in literature. Influent and effluent event-based

concentrations for dissolved and PM-based phosphorus are shown in Figure 3-9. The major source of phosphorus in the watershed is biogenic material, from leaf fall and grass-cutting maintenance, deposited on the pavement and mobilized during rainfall-runoff events.

Probability density functions (pdfs) for TDP, suspended P, settleable P, sediment P, and TP are provided for influent and effluent samples based on all 25 monitored events. The measured distributions are illustrated in Figure 3-10. All of the measured results for both influent and effluent samples are log-normally distributed at a 0.05 significance level with an R-squared greater than 0.85. Mann-Whitney rank sum tests are conducted on dissolved and particulate-bound fractions to compare influent and effluent results. Results of the tests indicate that, for all particulate-bound phosphorus fractions as well as TP, the effluent concentrations are significantly lower ($p \leq \alpha = 0.05$) than the influent. However, there is no significant difference ($p > \alpha = 0.05$) between influent and effluent dissolved phosphorus. This is partly because there is no mechanism in the treatment unit to remove dissolved nutrients, but it is also because, during the time between treated storm events, phosphorus bound to the PM retained in the unit is resuspending into the dissolved phase and leaving the unit as part of the effluent during events. This indicates that regular maintenance for the unit is required to periodically collect PM trapped in the unit during treatment.

Conclusion

The VCF unit evaluated in this study shows significant removal capabilities for both PM and particulate-bound phosphorus. Coarse particles (sediment PM) are removed with the highest volume-weighted mean efficiency of 100%. Fine particles (settleable and suspended PM) are also significantly removed with a volume-weighted mean removal efficiency of 87%. The volume-weighted mean removal efficiency of total PM (as SSC) is 98%. The median influent d_{50} for this study is 82 µm and the median effluent d_{50} is 3 µm. A comparison of PM removal

and PSD between primary effluent (sedimentation only) and secondary effluent (sedimentation + filtration) demonstrated that filtration significantly increases the PM removal efficiency of the unit. The volume-weighted mean removal of SSC without filtration for the 25 monitored events is 87% and the median effluent d_{50} is 10 µm. Similar trends in removal of phosphorus are seen, with the highest removal efficiency occurring for sediment-bound P. The volume-weighted mean removal efficiencies for sediment P, settleable P, suspended P, and dissolved P are 99%, 94%, 40%, and 0%, respectively. The volume-weighted mean removal efficiency for total P is 68%.

Table 3-1. Monitored rainfall-runoff event characteristics

Event Date	**PDH** (hr)	**IPRT** (min)	$\mathbf{d_{rain}}$ (min)	$\mathbf{h_{rain}}$ (mm)	$\mathbf{i_{rain\text{-}max}}$ (mm/hr)	**c**	$\mathbf{V_i}$ (L)	$\mathbf{V_e}$ (L)	$\mathbf{Q_{max}}$ (L/s)	$\mathbf{Q_{med}}$ (L/s)	$\mathbf{Q_{mean}}$ (L/s)
28 May (2010)	96	10	112	20.6	76.2	0.73	7465	1849	4.3	1.0	1.1
16 June	20	18	61	16.0	61.0	0.63	5006	4760	5.4	0.7	2.2
21 June	42	6	43	23.4	121.9	0.74	8695	8517	7.5	5.5	5.1
30 June	24	8	50	13.2	76.2	0.83	5459	5342	9.1	3.3	4.0
15 July	75	8	28	9.7	91.4	0.75	3608	3310	13.3	1.4	3.1
1 August	24	5	36	30.0	127.0	0.80	11973	11616	14.3	4.7	5.5
6 August	120	12	104	3.6	50.8	0.78	1357	1101	6.8	0.1	0.3
7 August	24	7	48	8.6	50.8	0.61	2622	2513	13.3	0.4	0.9
23 August	48	20	42	2.8	5.1	0.22	312	177	1.3	0.1	0.1
12 September	141	17	52	6.9	50.8	0.48	1643	1503	3.9	0.1	0.5
26 September	40	11	78	3.6	5.1	0.63	1129	701	0.5	0.3	0.2
27 September	10	20	388	15.2	101.6	0.50	3841	3729	10.9	0.1	0.2
4 November	36	5	43	4.8	25.4	0.41	994	490	3.5	0.1	0.4
16 November	286	8	34	3.3	25.4	0.18	305	155	1.8	0.1	0.1
5 January	72	3	125	21.3	106.7	0.54	5800	4866	7.4	0.2	1.1
10 January	106	3	26	5.1	91.4	0.44	1129	1098	3.3	0.1	0.4
25 January	365	7	389	38.9	17.0	0.56	12406	12289	3.0	0.6	0.7
7 February	12	7	306	32.8	30.5	0.81	13229	13100	2.2	0.8	0.7
9 March	79	10	691	29.2	16.2	0.69	10551	9744	3.1	0.1	0.2
28 March	438	7	66	2.5	33.9	0.41	522	497	1.0	0.1	0.1
30 March	48	33	179	15.5	76.2	0.49	3766	3732	5.6	0.1	0.3
20 April	196	9	61	3.6	15.2	0.12	205	116	3.3	0.1	0.1
14 May	188	5	295	50.3	137.2	0.43	10802	10596	11.5	0.1	0.6
6 June	541	19	69	4.1	22.9	0.47	960	712	1.6	0.1	0.2
27 June (2011)	88	3	50	11.4	42.9	0.59	3383	2341	3.4	0.1	2.0
Mean	125	10	135	15.1	58.4	0.55	4686	4194	5.7	0.8	1.2
Median	75	8	61	11.4	50.8	0.56	3608	2513	3.9	0.1	0.5
SD	141	7	160	12.9	40.1	0.20	4286	4246	4.2	1.5	1.6

Table 3-2. Summary of event-based values for PM fractions

Event Date	Turbidity		Suspended PM (< 25 µm)			Settleable PM			Sediment PM (>75 µm)			SSC (all PM fractions)			% Volatile	
	EMV_i (NTU)	EMV_e (NTU)	EMV_i [mg/L]	EMV_e [mg/L]	ΔM (%)	EMV_i [mg/L]	EMV_e [mg/L]	ΔM (%)	EMV_i [mg/L]	EMV_e [mg/L]	ΔM (%)	EMV_i [mg/L]	EMV_e [mg/L]	ΔM (%)	EMV_i (%)	EMV_e (%)
28 May (2010)	35.6	14.1	43.7	11.9	87	45.4	6.9	93	435.9	6.2	99	532.2	15.4	99	51.0	40.2
16 June	32.7	10.7	40.2	19.7	53	39.6	2.0	95	788.4	7.0	99	1401.7	18.1	99	65.1	26.4
21 June	4.7	3.0	18.4	9.9	48	29.7	1.8	94	2328.4	5.6	100	1162.9	7.4	99	78.7	28.4
30 June	9.8	6.5	12.2	5.8	53	13.0	1.6	88	318.3	8.0	98	444.5	5.4	99	84.1	33.1
15 July	31.2	7.1	23.7	6.9	73	68.1	1.4	98	937.8	5.1	100	812.2	8.4	99	74.7	65.9
1 August	14.8	3.9	18.5	6.9	64	111.7	8.7	93	243.0	4.8	98	245.1	7.7	97	70.5	52.7
6 August	51.9	1.4	48.0	12.1	82	29.5	2.9	93	390.4	13.2	98	308.4	7.3	98	51.3	3.0
7 August	15.6	3.8	13.1	7.0	49	32.2	5.2	85	222.5	1.6	99	115.8	13.9	89	42.3	31.0
23 August	46.6	5.3	38.3	5.0	92	35.9	3.2	95	459.5	2.9	100	555.8	4.7	100	69.1	46.9
12 September	27.9	3.6	45.2	11.6	76	46.0	4.1	92	110.5	2.7	98	261.5	5.8	98	56.3	40.7
26 September	21.4	3.3	11.2	2.2	85	5.1	2.4	65	1262.4	8.7	100	117.9	5.0	97	58.5	80.0
27 September	14.1	5.1	44.5	5.0	89	50.0	2.1	96	874.1	3.2	100	765.1	6.8	99	55.1	37.9
4 November	82.5	5.5	93.6	6.7	96	51.5	3.0	97	486.6	4.2	100	477.1	9.6	99	46.2	53.0
16 November	171.0	10.8	123.2	9.4	96	137.8	2.4	99	332.2	19.7	97	543.6	12.2	99	43.5	10.7
5 January	65.7	10.1	68.6	13.0	84	83.6	2.9	97	1411.7	3.2	100	693.2	8.7	99	69.4	52.2
10 January	38.0	3.3	20.8	3.1	86	60.0	3.6	95	453.0	1.4	100	211.1	3.0	99	68.0	24.8
25 January	28.2	6.8	32.3	3.5	89	37.5	3.6	91	390.9	2.0	100	105.8	4.2	96	68.1	34.8
7 February	30.0	5.9	20.4	4.4	79	14.4	0.9	94	639.7	2.5	100	438.3	7.6	98	75.8	54.5
9 March	19.4	2.4	21.9	8.8	62	10.6	1.3	88	69.6	1.9	97	78.2	2.8	97	57.8	31.2
28 March	61.8	3.5	48.9	9.8	84	19.5	2.9	88	101.1	2.9	98	102.8	5.6	96	54.6	19.7
30 March	70.7	4.6	44.9	5.1	89	59.6	2.2	96	667.5	1.0	100	443.7	7.3	98	60.2	5.6
20 April	112.2	2.4	65.7	7.9	93	78.0	3.5	98	254.6	2.3	100	921.7	6.1	100	44.7	22.8
14 May	19.9	5.6	33.9	11.3	67	43.2	1.2	97	602.5	0.7	100	487.3	5.3	99	66.0	10.2
6 June	38.4	3.7	54.2	10.6	85	31.4	2.6	94	313.1	1.1	100	237.5	9.0	97	54.9	25.4
27 June (2011)	63.8	3.4	54.3	10.1	83	77.1	2.6	97	586.7	5.2	99	591.7	9.8	98	81.3	3.8
Mean	44.3	5.4	41.6	8.3	78	48.4	3.0	93	587.2	4.7	99	482.2	7.9	98	61.9	33.4
Median	32.7	4.6	40.2	7.9	84	43.2	2.6	94	453.0	3.2	100	444.5	7.3	99	60.2	31.2
SD	36.7	3.1	26.3	3.9	15	31.5	1.8	7	494.7	4.3	1	338.4	3.7	2	12.1	19.6

Table 3-3. Comparison of event-based PM indices of d_{10}, d_{50}, and d_{90} for influent, primary effluent, and secondary effluent

Event Date	Measured influent PSD (µm)			Primary effluent PSD (after settling) (µm)			Measured secondary effluent PSD (settling + filtration) (µm)		
	d_{10}	d_{50}	d_{90}	d_{10}	d_{50}	d_{90}	d_{10}	d_{50}	d_{90}
28 May (2010)	7	69	915	5	16	34	2	11	34
16 June	28	242	1016	4	17	38	1	6	16
21 June	54	263	769	6	21	44	1	6	34
30 June	8	75	271	2	14	54	1	5	17
15 July	40	225	628	5	23	53	2	6	17
1 August	26	213	693	4	25	67	2	6	17
6 August	16	231	984	3	12	40	1	3	18
7 August	19	186	737	2	9	37	1	4	12
23 August	14	190	714	2	6	17	2	4	40
12 September	9	89	328	3	11	25	1	2	8
26 September	4	35	173	1	4	11	1	3	52
27 September	15	136	723	2	14	47	1	3	11
4 November	3	68	401	1	6	21	1	2	9
16 November	5	51	610	1	6	18	1	2	12
5 January	15	110	794	2	12	36	1	3	12
10 January	8	117	227	1	6	23	1	2	6
25 January	7	63	308	1	8	27	0	1	2
7 February	7	68	369	2	8	23	1	3	18
9 March	6	57	278	2	5	14	1	3	7
28 March	4	32	200	1	3	8	1	3	8
30 March	6	44	176	2	10	35	1	3	7
20 April	2	22	310	1	4	14	0	1	8
14 May	10	80	705	2	12	36	1	3	8
6 June	10	99	345	2	8	19	1	2	7
27 June (2011)	10	82	310	2	11	29	1	6	14
Mean	13	114	519	2	11	31	1	4	16
Median	9	82	401	2	10	29	1	3	12
SD	12	74	270	1	6	15	0	2	12

Table 3-4. Comparison of event-based SSC for influent, primary effluent, and secondary effluent

Event Date	Influent	Primary effluent (after settling)		Measured secondary effluent (settling + filtration)	
	SSC [mg/L]	**SSC** [mg/L]	**ΔM** (%)	**SSC** [mg/L]	**ΔM** (%)
28 May (2010)	532.2	51.8	90	15.4	99
16 June	1401.7	68.3	88	18.1	99
21 June	1162.9	12.6	99	7.4	99
30 June	444.5	158.5	65	5.4	99
15 July	812.2	147.0	82	8.4	99
1 August	245.1	42.2	83	7.7	97
6 August	308.4	49.7	84	7.3	98
7 August	115.8	14.3	88	13.9	89
23 August	555.8	39.7	93	4.7	100
12 September	261.5	27.5	89	5.8	98
26 September	117.9	9.9	92	5.0	97
27 September	765.1	72.0	91	6.8	99
4 November	477.1	127.4	75	9.6	99
16 November	543.6	90.4	84	12.2	99
5 January	693.2	99.6	86	8.7	99
10 January	211.1	12.4	76	3.0	99
25 January	105.8	28.7	88	4.2	96
7 February	438.3	38.0	92	7.6	98
9 March	78.2	29.9	83	2.8	97
28 March	102.8	16.0	84	5.6	96
30 March	443.7	12.6	98	7.3	98
20 April	921.7	100.4	90	6.1	100
14 May	487.3	70.9	85	5.3	99
6 June	237.5	43.2	82	9.0	97
27 June (2011)	471.3	103.7	78	9.8	98
Mean	477.4	58.7	86	7.9	98
Median	444.5	43.2	86	7.3	99
SD	337.6	43.8	7	3.7	2

Table 3-5. Comparison of event-based gamma parameters for influent, primary effluent, and secondary effluent

Event Date	Influent PSD		Primary effluent PSD (after settling)		Measured secondary effluent PSD (settling + filtration)	
	k	λ	k	λ	k	λ
28 May (2010)	0.45	295.2	2.00	9.2	1.19	12.9
16 June	0.86	427.9	1.58	12.9	1.44	5.3
21 June	1.29	291.3	1.83	13.0	1.21	7.6
30 June	0.77	155.0	0.82	26.8	1.08	8.1
15 July	1.02	240.6	1.54	17.5	0.91	14.7
1 August	1.01	337.8	1.17	27.5	1.29	6.4
6 August	0.60	579.0	1.17	14.2	0.83	5.8
7 August	0.74	404.3	1.10	12.2	1.31	3.7
23 August	0.71	399.1	1.39	5.5	0.68	23.0
12 September	0.65	401.7	1.58	8.3	1.81	2.1
26 September	0.66	130.6	1.57	3.3	0.65	15.9
27 September	0.73	414.3	0.79	26.6	1.24	4.4
4 November	0.51	212.2	1.15	7.5	1.94	1.6
16 November	0.53	461.6	1.27	6.6	0.47	46.3
5 January	0.56	487.7	1.13	14.9	1.39	3.7
10 January	0.80	146.1	1.08	8.4	1.99	1.6
25 January	0.85	174.5	1.00	11.4	1.29	6.1
7 February	0.61	234.0	1.37	7.5	0.20	34.8
9 March	0.64	370.7	1.68	3.8	1.39	2.8
28 March	0.62	155.9	1.74	2.0	2.01	1.7
30 March	0.59	453.8	0.95	16.2	0.83	4.2
20 April	0.45	493.0	1.31	4.5	0.52	6.9
14 May	0.63	300.5	0.99	16.5	1.68	2.0
6 June	0.71	294.0	1.51	6.2	0.23	14.9
27 June (2011)	0.88	140.3	1.26	11.4	0.62	33.7
Mean	0.71	320.0	1.32	11.8	1.13	10.8
Median	0.66	300.5	1.27	11.4	1.21	6.1
SD	0.19	130.4	0.32	7.2	0.53	11.8

Table 3-6. Summary of event-based values for dissolved and particulate-bound phosphorus

Event Date	Dissolved P (DP) fraction			Suspended P (1 to 25 µm)			Settleable P			Sediment P (>75 µm)			Total P (Σ all fractions)		
	EMV_i [µg/L]	EMV_e [µg/L]	ΔM (%)	EMV_i [µg/L]	EMV_e [µg/L]	ΔM (%)	EMV_i [µg/L]	EMV_e [µg/L]	ΔM (%)	EMV_i [µg/L]	EMV_e [µg/L]	ΔM (%)	EMV_i [µg/L]	EMV_e [µg/L]	ΔM (%)
28 May (2010)	498	362	64	714	359	75	175	26	93	1025	15	99	2405	762	84
16 June	328	318	8	444	402	32	266	13	95	2218	20	99	3256	666	81
21 June	175	229	0	116	112	6	103	6	94	5489	13	100	5883	360	94
30 June	216	249	0	265	172	37	76	9	88	660	17	98	1216	447	64
15 July	638	453	35	319	258	26	357	7	98	2234	12	99	3548	731	81
1 August	193	402	0	566	468	20	407	31	93	1175	23	98	2342	920	62
6 August	665	521	43	343	363	23	11	1	93	1021	35	98	2040	920	67
7 August	199	318	0	588	607	1	166	27	84	454	3	99	1407	955	35
23 August	527	655	23	472	232	69	19	2	95	592	4	100	1570	883	65
12 September	690	1045	0	753	237	71	21	2	92	671	17	98	2135	1300	44
26 September	669	854	6	562	591	23	11	5	65	1825	13	99	3068	1463	65
27 September	496	714	0	1218	1008	19	70	3	96	1279	5	100	3063	1730	45
4 November	1437	1030	64	1979	1347	66	355	21	97	1240	11	100	5011	2409	76
16 November	1921	1598	55	2619	787	84	1470	25	99	2891	165	97	8793	2574	84
5 January	1059	1360	0	820	733	23	171	5	98	1944	6	100	3947	2104	54
10 January	1036	1387	0	1106	1085	8	334	20	94	1378	4	100	3853	2496	39
25 January	450	507	0	1802	488	73	125	12	90	2120	11	99	4497	1146	75
7 February	684	626	9	706	546	23	13	1	94	1552	6	100	3407	1179	66
9 March	394	628	0	470	309	37	44	6	88	176	5	97	887	806	11
28 March	4670	2557	56	1780	1162	38	113	18	87	231	6	98	5718	3132	56
30 March	878	1111	0	1382	1196	14	255	9	96	1874	3	100	4364	2474	44
20 April	2045	4002	0	790	756	47	164	7	98	3505	3	100	6504	4769	59
14 May	740	790	0	618	685	0	128	3	98	1507	2	100	2994	1480	51
6 June	1177	1881	0	735	471	51	175	14	94	669	2	100	2769	2368	35
27 June (2011)	791	2182	0	830	557	37	370	13	97	1237	7	99	3228	2758	20
Mean	903	1031	15	880	597	36	216	11	93	1559	16	99	3516	1633	58
Median	669	714	0	714	546	32	164	9	94	1279	7	99	3228	1300	62
SD	925	876	23	608	342	25	290	9	7	1151	32	1	1825	1039	21

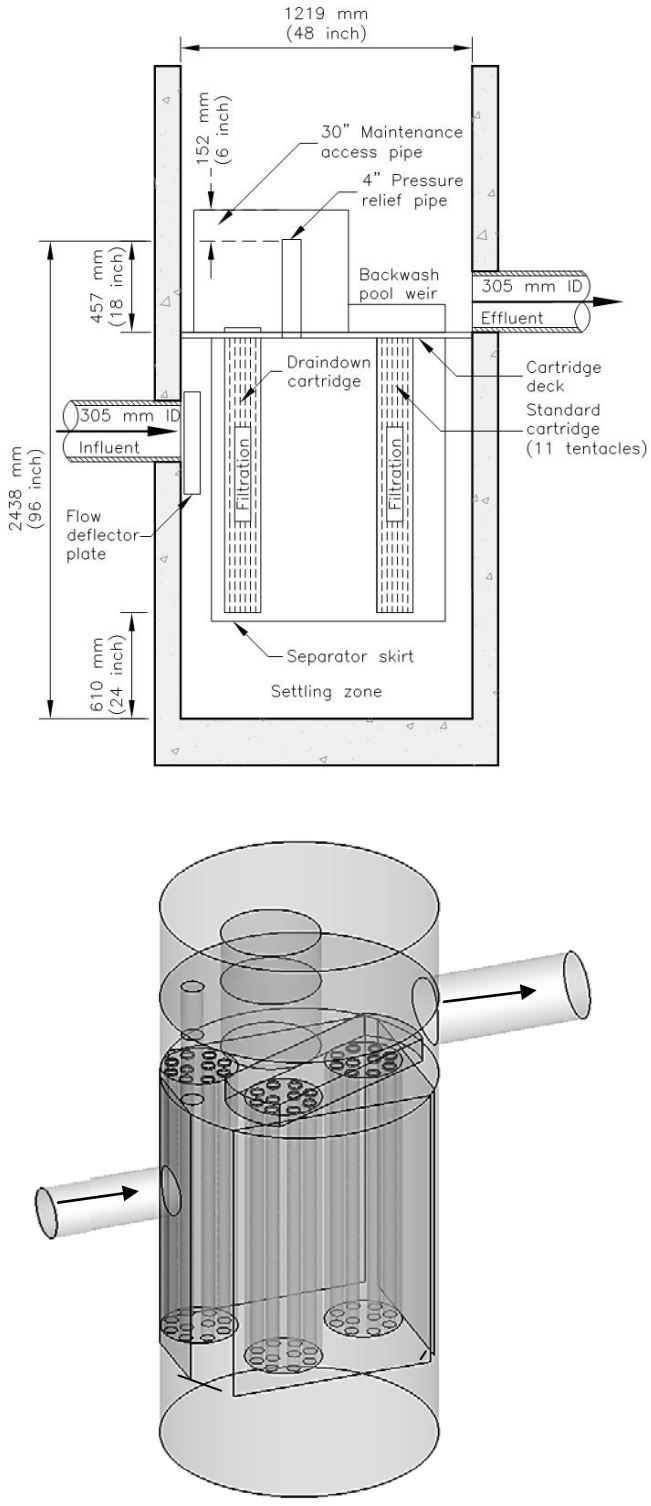

Figure 3-1. Volumetric clarifying filter treatment unit design

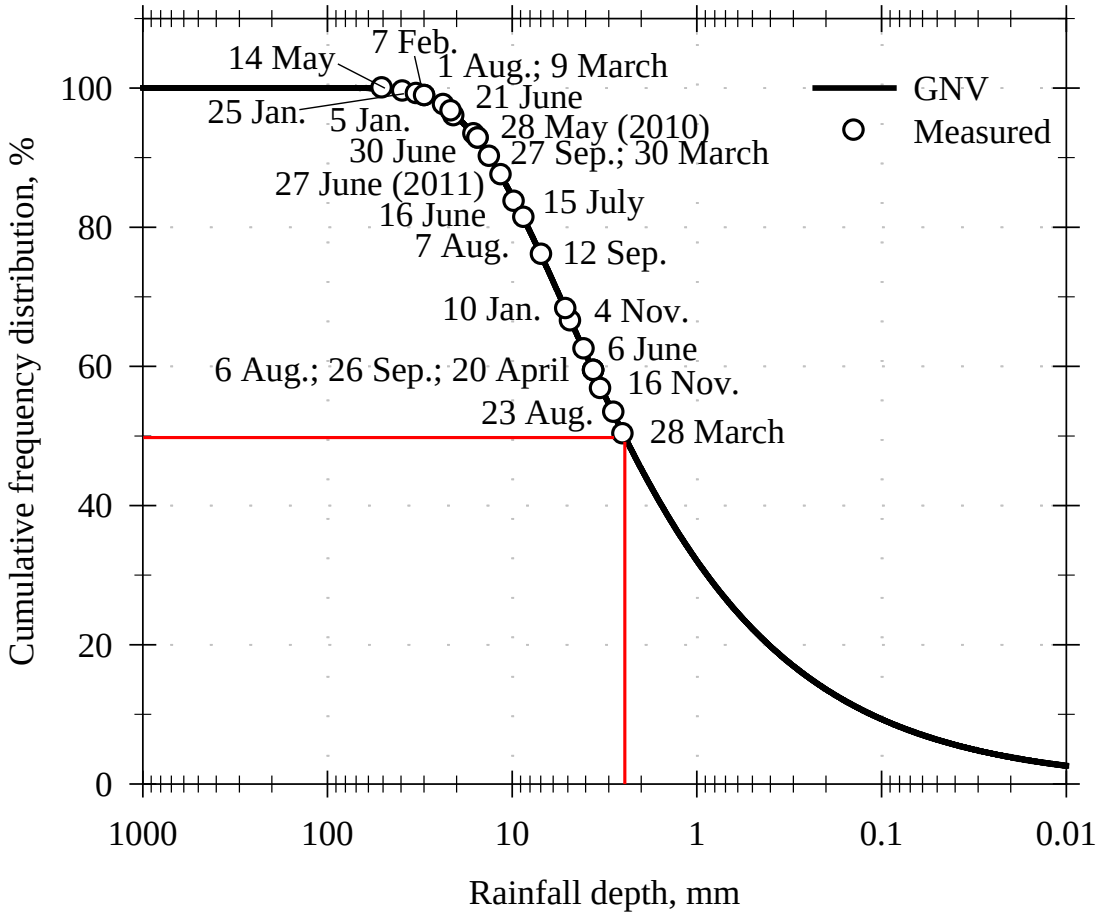

Figure 3-2. Cumulative frequency distribution of rainfall depth for Gainesville, FL (GNV) based on 30 years of rainfall data (1980-2010)

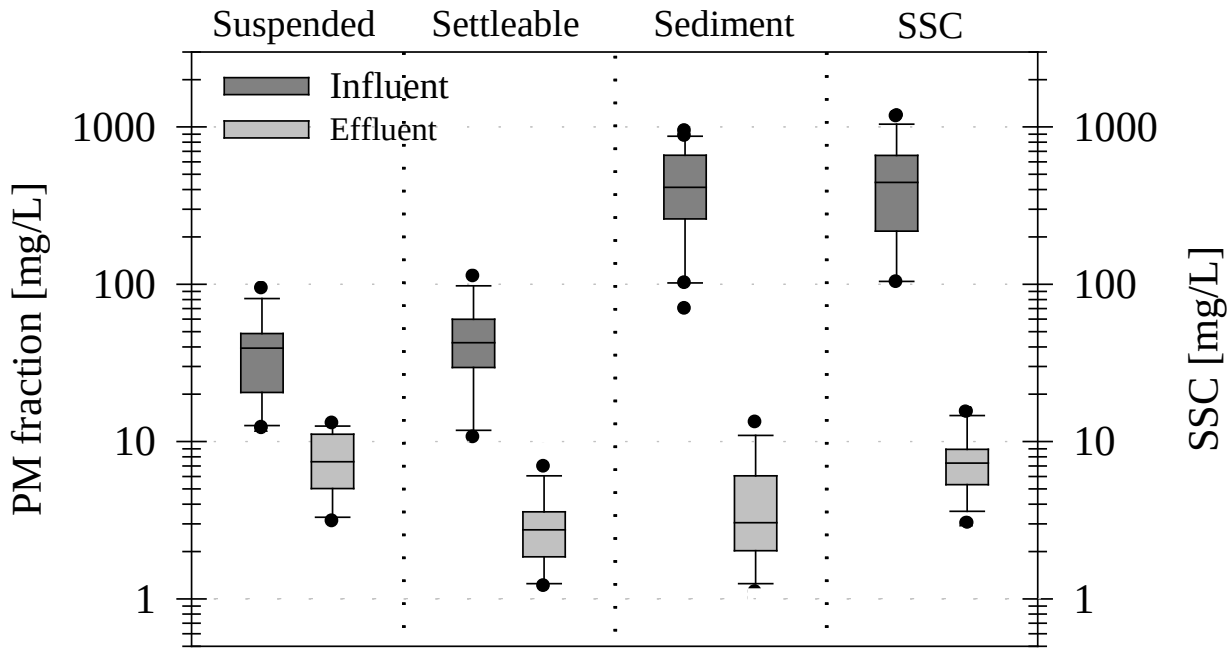

Figure 3-3. Suspended (< 25 µm), settleable (25 – 75 µm), sediment (> 75 µm) PM fractions and SSC (all PM fractions) for influent and effluent

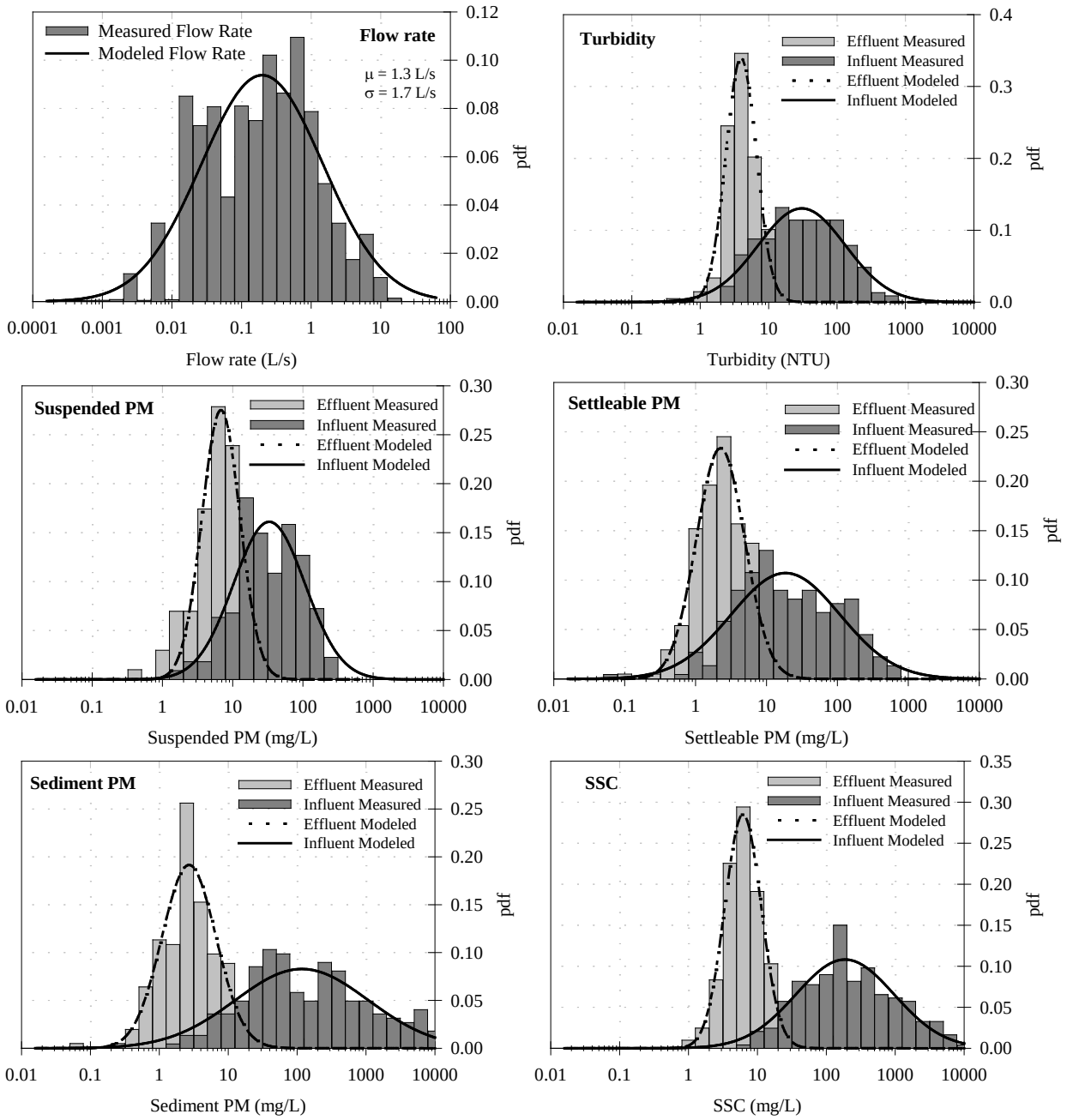

Figure 3-4. Probability density functions (pdfs) for flow rate, turbidity, and PM fractions ($p > \alpha = 0.05$)

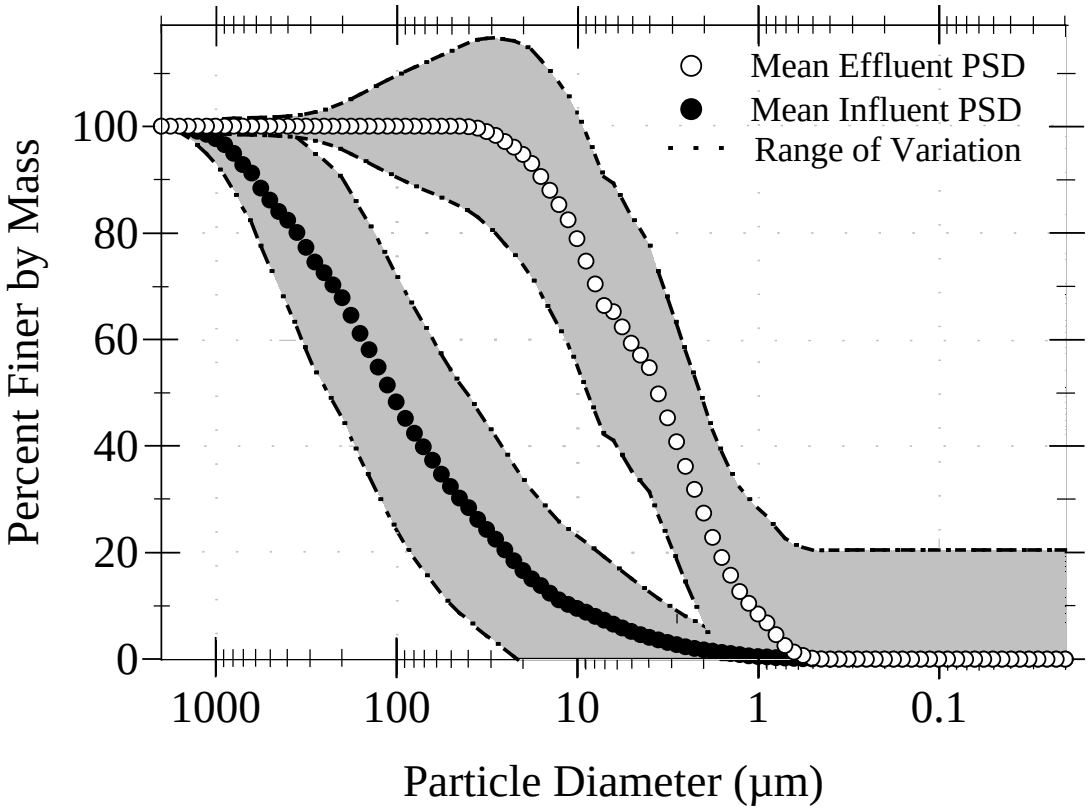

Figure 3-5. Median and range of variation for the influent and effluent PSD from the entire monitoring campaign (n=35)

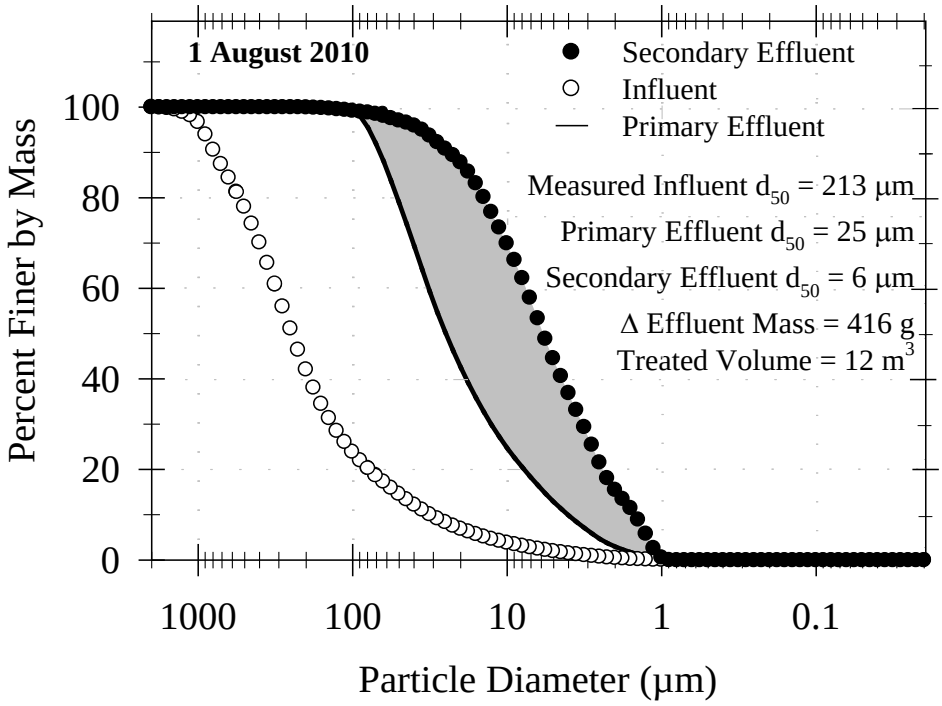

Figure 3-6. Measured influent and secondary effluent PSD and modeled primary effluent PSD for the 1 August 2010 event

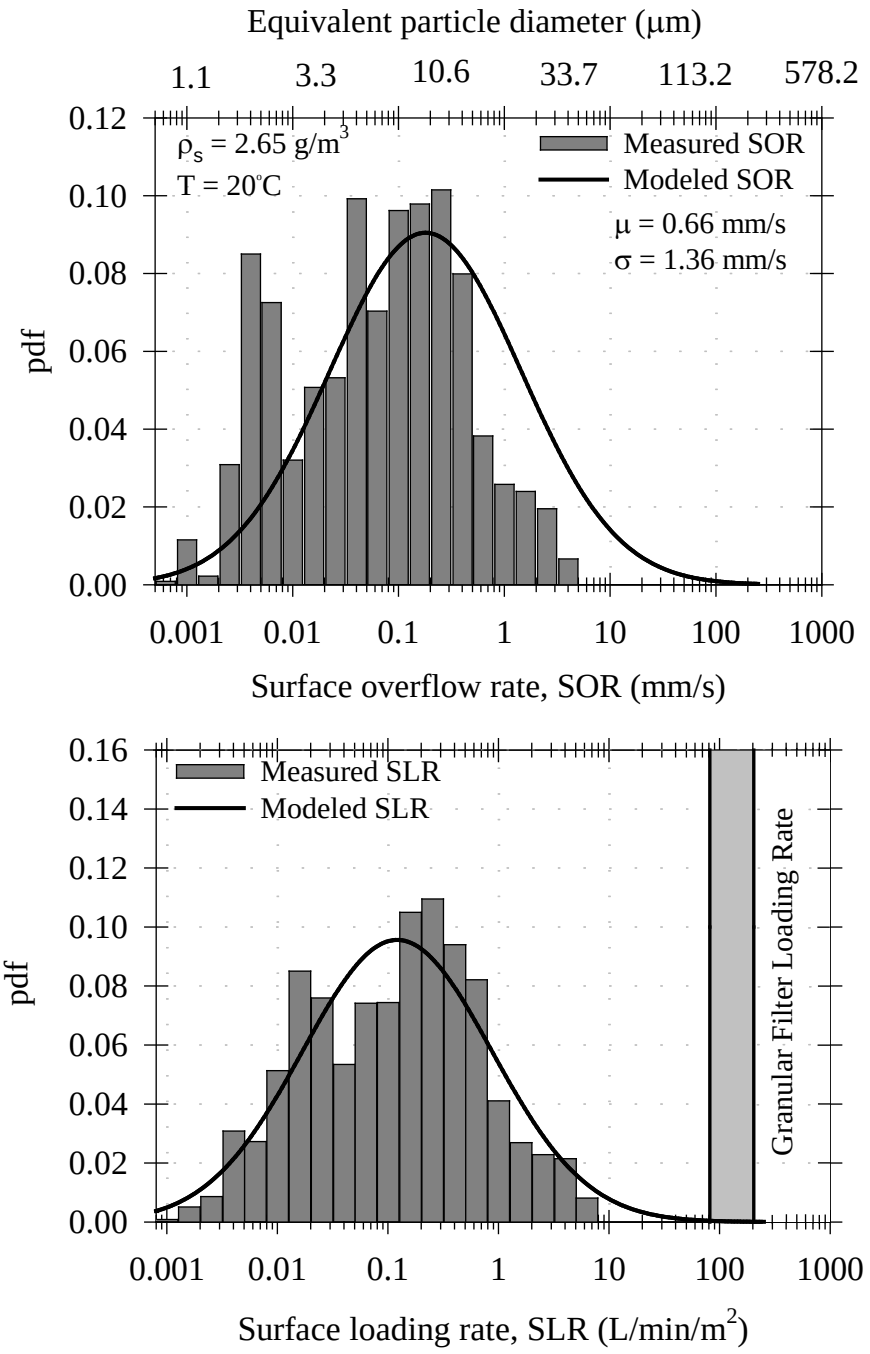

Figure 3-7. Probability density functions (pdfs) for surface overflow rate, SOR and surface loading rate, SLR ($p > \alpha = 0.05$)

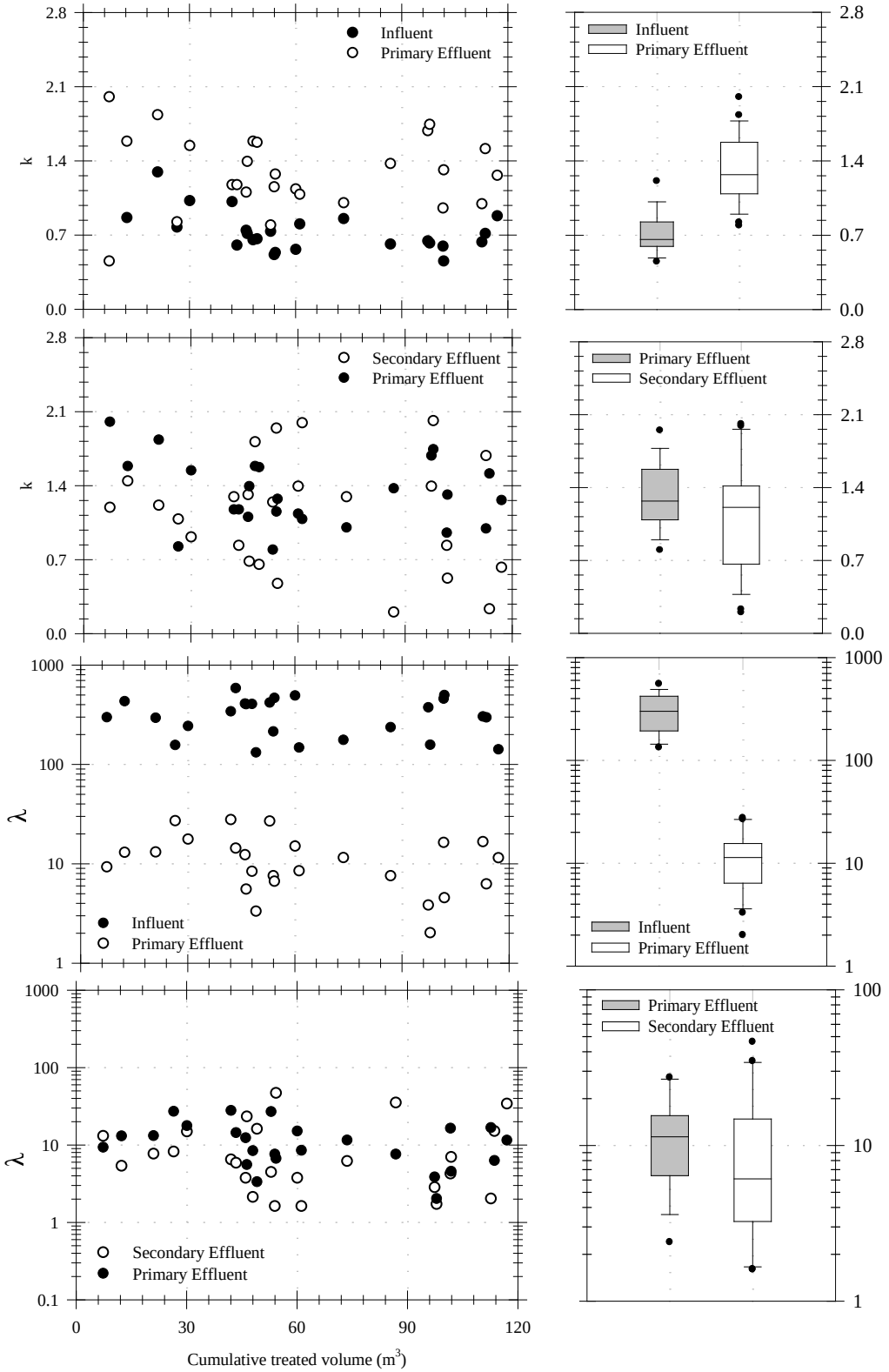

Figure 3-8. Event-based cumulative gamma distribution parameters for measured influent, modeled primary effluent, and measured secondary effluent PSD

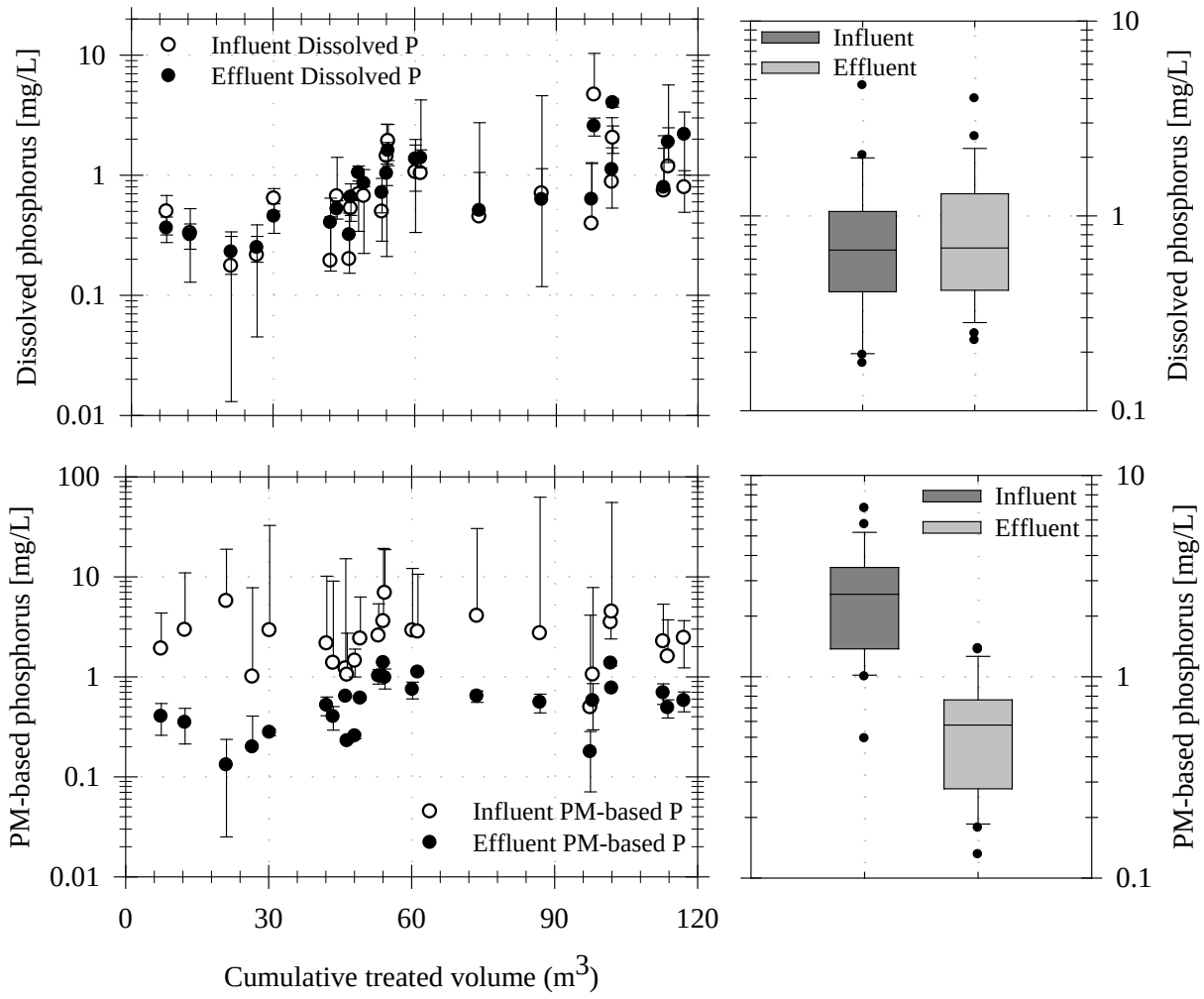

Figure 3-9. Event-based influent and effluent dissolved phosphorus and PM-based phosphorus

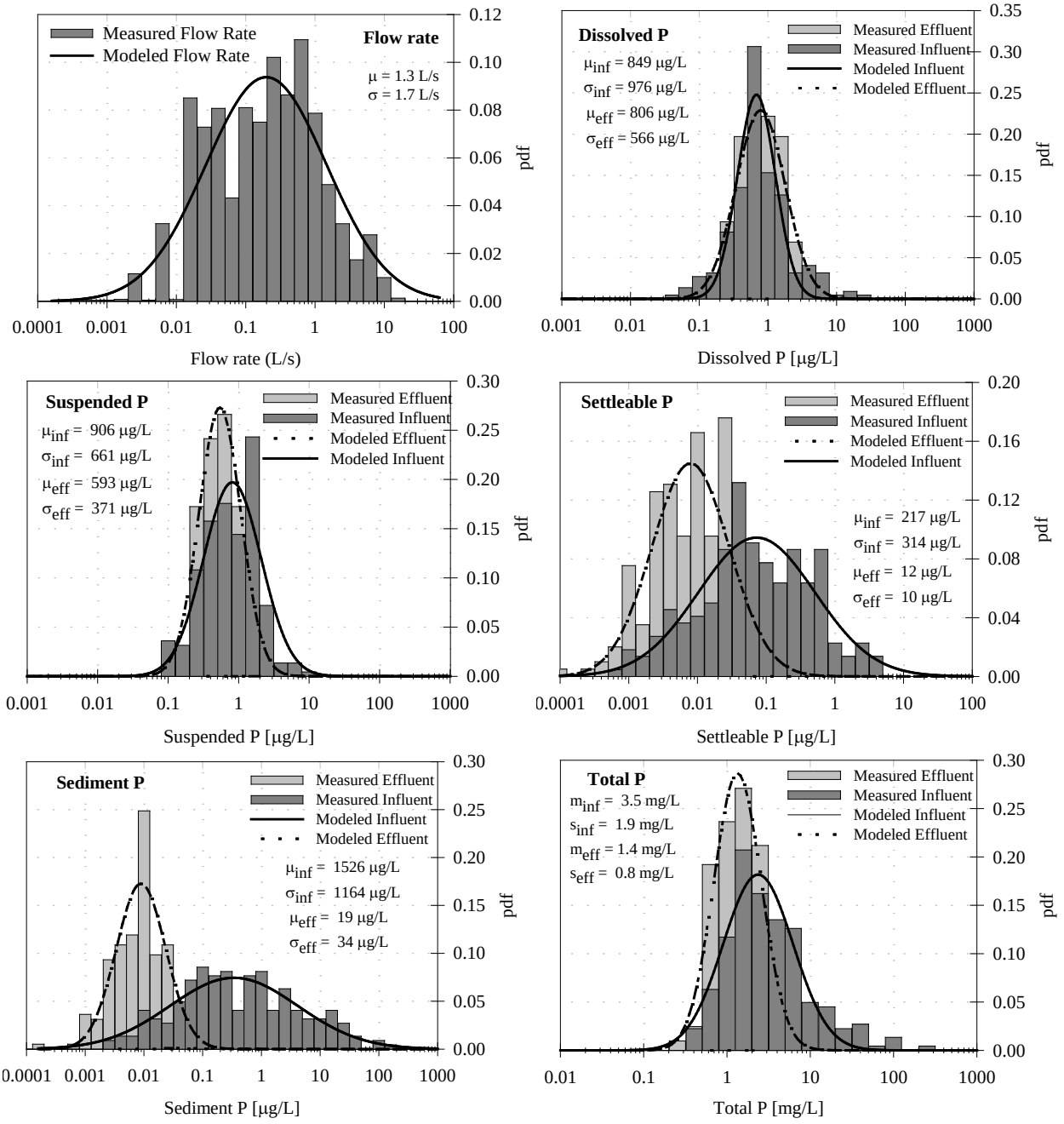

Figure 3-10. Probability density functions (pdfs) for flow rate and dissolved and particulate-bound phosphorus ($p > \alpha = 0.05$)

CHAPTER 4
GLOBAL SUMMARY AND CONCLUSIONS

This study evaluates the two primary sampling techniques for rainfall-runoff monitoring to determine which provides a more representative PM analysis under various rainfall intensities, runoff durations, and PM loads. Monitoring is conducted on the Reitz Union parking facility located on the University of Florida campus in Gainesville, FL. PM from eight wet weather events was sampled in parallel using manual and automated sampling techniques and samples are analyzed for PSD, PND, SSC, and PM fractions. Also in this study, the treatment efficiency of a volumetric clarifying filter (VCF) unit is assessed under various rainfall intensities, runoff durations, and PM loads. Manual grab samples are taken during 25 wet weather events and samples are analyzed for PM fractions, like sediment PM, settleable PM, TSS, and SSC, PSD, and dissolved and particulate-bound phosphorus. Influent and effluent event mean concentrations are calculated along with removal efficiencies to assess treatment capabilities. This chapter summarizes the conclusions reached in this study.

Results of the analyses on sampling techniques indicate that there are statistically significant differences between a PM analysis using manual sampling and one using automated sampling. For a size heterodisperse runoff with a median particle diameter (by mass) above 159 µm, samples taken with an automated sampler significantly underestimate the PM load. This indicates that manual grab sampling paired with the SSC method and PSD characterization is a more accurate PM analysis for most untreated urban rainfall-runoff from small watersheds. On the contrary, for runoff containing mostly fine particles (< 75 µm), this is not the case. For size monodisperse runoff with a d_{50} (by mass) below 159 µm, there is no significant difference between the two PM analyses. This indicates that either sampling technique representatively characterizes the treated effluent from a rainfall-runoff treatment unit implementing

sedimentation with or without filtration. A preliminary PM analysis is required in this case to determine if the effluent is truly size monodisperse and composed of fine particles smaller than 159 µm.

There are two main constraints of automated samplers that are responsible for the difficulties associated with stormwater monitoring. The first is that they do not sample the entire depth of flow. The location of the intake tube within the depth of flow greatly impacts sampling, since higher concentrations of particles are found at lower depths. The second is that the uptake velocity of the automated sampler is usually not equal to the localized streamflow velocity. Runoff flow rates are not constant; however intake tube uptake velocities are fixed. This leads to mostly non-isokinetic sampling and substantial error due to inertial effects of the particles.

Results of the VCF treatment assessment indicate that this unit shows significant removal capabilities for both PM and particulate-bound phosphorus. Coarse particles (> 75 µm) are removed with the highest volume-weighted mean efficiency of 100%. Fine particles (< 75 µm) are also significantly removed ($p \leq \alpha = 0.05$) with a volume-weighted mean removal efficiency of 87%. The volume-weighted mean removal efficiency of total PM (as SSC) is 98%. The median influent particle diameter for this study is 82 µm and the median effluent particle diameter is 3 µm. A comparison between both measured mass load reduction and effluent PSD for the VCF and a modeled mass load reduction and effluent PSD for a treatment unit of the same size without filtration demonstrated that filtration significantly increases the PM removal efficiency of the unit. The volume-weighted mean removal of SSC by a unit with hydrodynamic separation alone for the 25 monitored events is 87% and the median effluent particle diameter is 10 µm. Similar trends in removal of phosphorus are seen, with the highest volume-weighted mean removal efficiency of 99% occurring for sediment-bound P. All other particulate-bound

phosphorus fractions are significantly lower ($p \leq \alpha = 0.05$) in the effluent than in the influent. The volume-weighted mean removal efficiency for total P is 68%. However, there is no significant decrease ($p > \alpha = 0.05$) in dissolved phosphorus concentration in the effluent as compared to the influent.

LIST OF REFERENCES

Andral, M.C., Roger, S., Montrjaud-Vignoles, M., Herremans, L., 1999. Particle size distribution and hydrodynamic characteristics of solid matter carried by runoff from motorways. Water Environment Research 71 (4), 398-407.

American Society for Testing and Materials (ASTM), 1997. Standard methods for determining sediment concentration in water. Annual Book of ASTM Standards, Designation D3977-97(B). ASTM, West Conshohocken, PA.

Bader, H., 1970. The hyperbolic distribution of particle sizes. Journal of Geophysical Research 75 (15), 2822-2830.

Barrett, M.E., Irish, L.B., Jr., Malina, J.F., Jr., Charbeneau, R.J., 1998. Characterization of highway runoff in Austin, Texas area. Journal of Environmental Engineering 124 (2), 131-137.

Bent, G.R., Gray, J.R., Smith, K.P., Glysson, G.D., 2001. A synopsis of technical issues for monitoring sediment in highway and urban runoff. U.S. Geological Survey Open-File Report 00497. U.S. Geological Survey.

Brown, P.A., Gill, S.A., Allen, S.J., 2000. Metal removal from wastewater using peat. Water Research 16, 3907-3916.

Burton, G.A., Pitt, R., 2001. Stormwater Effects Handbook: A Toolbox for Watershed Managers, Scientists, and Engineers. Lewis Publishers, Boca Raton, FL. 928 pages.

Clark, S.E., 2000. Urban stormwater filtration: Optimization of design parameters and a pilot-scale evaluation. *PhD dissertation*, University of Alabama at Birmingham, Birmingham, Alabama.

Clark, S.E., Siu, C.Y.S., 2007. Measuring solids concentration in stormwater runoff: comparison of analytical methods. Environmental Science and Technology 42(2), 511-516.

Clark, S. E., Siu, C. Y. S., Roenning, C. D., Treese, D. P., Pitt. R., Bathi, J. R., 2007. Automatic sampler efficiency for stormwater solids. Presented at the 2007 Pennsylvania Stormwater Management Symposium. Villanova, PA. October 18, 2007.

Colorado Department of Public Health and Environment, 1996. CDPS Stormwater Sampling Guidance Document.

Corell, D. L., 1998. The role of phosphorus in the eutrophication of receiving waters: a review. Journal of Environmental Quality 27, 261-266.

Cristina, C., Tramonte, J., Sansalone, J.J., 2002. A granulometry-based selection methodology for separation of traffic-generated particles in urban highway snowmelt runoff. Water, Air, and Soil Pollution 136, 33-53.

Cristina, C., Tramonte, J.J., Cartledge, F.K., Pardue, J.H., 2005. Influence of hydrology on rainfall-runoff metal element speciation. Journal of Environmental Engineering-ASCE 131(4), 632-642.

De Leon, D.B., Lowe, J., 2009. Washington State Department of Ecology Standard Operating Procedure for Automatic Sampling for Stormwater Monitoring.

Dickenson, J.A., Sansalone, J.J., 2009. Discrete phase model representation of particulate matter (PM) for simulating PM separation by hydrodynamic unit operations. Environmental Science and Technology 43 (21), 8220-8226.

Dizer, H., Grutzmacher, G., Bartel, H., Wiese, H.B., Szewzyk, R., and Lopez-Pila, J.M., 2004. Contribution of the colmation layer to the elimination of coliphages by slow sand filtration. Water Science and Technology 50 (2) 210-214.

EPA, 1992. NPDES Storm Water Sampling Guidance Document.

EPA, 2000. 2000 National Water Quality Inventory. National Water Quality Report to Congress under Clean Water Act Section 305(b) http://www.epa.gov/305b/2000report/ (last accessed January 11, 2011).

Furamai, H., Balmer, H., Boller, M., 2002. Dynamic behavior of suspended pollutants and particle size distribution in highway runoff. Water Science and Technology 46(11-12), 413-418.

Glenn, T., Tribouillard, S., Mishra, S., Singh, V., Sansalone, J., 2001. Pollutant mass and physical particulate pollution as a function of particle size and traffic for urban snow runoff, *NOVATECH Conference Proceedings*, Lyon, Frankreich, 945-952.

Gnecco, I., Berretta, C., Lanza, L.G., La Barbera, P., 2005. Storm water pollution in the urban environment of Genoa, Italy. Atmospheric Research 77 (1-4), 60-73.

Gobel, P., Dierkes, C., Coldeway, W.G., 2007. Storm water runoff concentration matrix for urban areas. Journal of Contaminant Hydrology 91 (1-2), 26-42.

Gray, J.R., Glysson, G.D., Turcios, L.M., Schwartz, G.E., 2000. Comparability of suspended-sediment concentration and total suspended solids data. U.S. Dept. of the Interior, USGS Information Services, Reston, Virginia.

Greb, S.R., Bannerman, R.T., 1997. Influence of particle size on wet pond effectiveness. Water Environment Research 69 (6), 1134-1138.

Grizzard, T.L., Randall, C.W., Weand, B.L., Ellis, K.L., 1986. Effectiveness of extended detention ponds, pp. 323 – 337. *In* Urbonas, B., and Roesner, L.A., Urban runoff quality- Impact of quality enhancement technology. ASCE, New York.

Grottker, M., 1987. Runoff quality from a street with medium traffic loading. Science of the Total Environment 59, 457-466.

Harmel, R.D., King, K.W., Slade, R.M., 2003. Automated storm water sampling on small watersheds. Applied Engineering in Agriculture, 19 (6), 667-674.

James, R.B., 2003. TSS: A viable neasure of storm water pollutants? Proceedings of the 1st Annual North American Surface Water Quality Conference and Exposition, StormCon 2003, San Antonia, TX. Avaliable at http://204.202.251.206/assets/55TSS.pdf (accessed on March 14, 2011).

Khan, S., Lau, S.L., Kayhanian, M., Stenstrom, M.K., 2006. Oil and grease measurement in highway runoff: sampling time and event mean concentrations. Journal of Environmental Engineering 132, 415-422.

Lau, S.L., Stenstrom, M.K., 2005. Metals and PAHs adsorbed to street particles. Water Research 39, 4083-4092.

Lawson, T.B., 1994. Fundamentals of aquacultural engineering. Kluwer Academic Publishers, Norwell.

Legret, M., Pagotto, C., 1999. Evaluation of pollutant loadings in the runoff waters from a major rural highway. Science of the Total Environment 235 (1-3), 143-150.

Lee, J.H., Bang, K.W., 2000. Characterization of urban stormwater runoff. Water Resources 34, 1773-1780.

Li, Y.X., Lau, S.L., Kayhanian, M., and Stenstrom, M.K., (2005). Particle size distribution in highway runoff. Journal of Environmental Engineering—ASCE 131 (9), 267-1276.

Liebens, J., 2001. Heavy metal contamination of sediments in stormwater management systems: The effect of land use, particle size, and age. Environmental Geology 41, 341-351.

Lin, H., Ying, G., Sansalone, J., 2009. Granulometry of non-colloidal particulate matter transported by urban runoff. Water Air Soil Pollution 198, 269-284.

Liu, B., Sansalone, J., Ying, G., 2010. Volumetric filtration of rainfall-runoff: (I) separation of particulate matter and filter forensics. Journal of Environmental Engineering 136 (12), 1321-1330.

Marsalek, J., Rochfurt, Q., Brownlee, B., Mayor, T., Servos, M., 1999. An exploratory study of urban runoff toxicity. Water Science and Technology 39 (12), 33-39.

Metcalf, L., Eddy, H., 2003. Wastewater Engineering: Treatment and Reuse. McGraw-Hill, Boston, MA.

Nix, S.J., Heaney, J.P., Huber, W.C., 1988. Suspended solids removal in detention basins. Journal of Environmental Engineering 114 (6), 1331-1341.

Pathapati, S., Sansalone, J.J., 2009. Combining particle analyses with computation fluid dynamics modeling to predict hetero-disperse particulate matter fate and pressure drop in a passive runoff radial filter. Journal of Environmental Engineering 135 (2), 77-85.

Pitt, R., S. Clark, P.D. Johnson, R. Morquecho, S. Gill, and Pratap, M., 2004. High level treatment of stormwater heavy metals. *Proceedings of the 2004 World Water and Environmental Resources Congress: Critical Transitions in Water and Environmental Resources Management*, Jun 27-Jul 1 2004, Salt Lake City, UT, 917-926.

Pratt, C.J., Mantle, J.D.G., Schofield, P.A., 1995. UK research into the performance of permeable pavement, reservoir structures in controlling stormwater discharge quantity and quality. Water Science and Technology 32 (1), 63-69.

Reed, G.D., 1981. Evaluation of Automatic Suspended Solids Sampling Procedures. Water Pollution Control Federation 53(10), 1481-149.

Roesner, L.A., 1999. Urban runoff pollution – summary thoughts – the state-of-practice today and for the 21st century. Water Science and Technology 39 (12), 353-360.

Roger, S., Montrejaud-Vignoles, M., Andral, M.C., Herremans, L., Fortune, J.P., 1998. Mineral, physical and chemical analysis of the solid matter carried by motorway runoff water. Water Research 32 (4), 1119-1125.

Rushton, B., England, G., Smith, D., 2007. ASCE guidelines for monitoring stormwater gross pollutants. The 9th biennial conference on stormwater research and watershed management. Orlando, Florida.

Sansalone, J.J., Buchberger, S.G., 1997. Characterization of solid and metal element distributions in urban highway stormwater. Water Science and Technology 36 (8-9), 155-160.

Sansalone, J.J., Buchberger, S.G., 1997. Partitioning and first flush of metals in urban roadway storm water. Journal of Environmental Engineering-ASCE 123(2), 134-143.

Sansalone, J.J., Cristina, C.M., 2004. Prediction of gradation-based heavy metal mass using granulometric indices of snowmelt particles. Journal of Environmental Engineering 130, 1488-1497.

Sansalone, J.J., Kim, J.Y., 2008. Transport of particulate matter fractions in urban source area pavement surface runoff. Journal of Environmental Quality 37, 1883-1893.

Sansalone, J.J., Koran, J.M., Smithson, J.A., Buchberger, S.G., 1998. Physical characteristics of urban roadway solids transported during rain events. Journal of Environmental Engineering-ASCE 124(5), 427-440.

Sartor, J.D., Boyd, G.B., Agardy, F.J., 1974. Water pollution aspects of street surface contaminants. Journal WPCF 46 (3), 458-467.

Standard Methods for the Examination of Water and Wastewater, 1995. American Public Health Association, Washington, DC.

State of Maine Bureau of Land and Water Quality Management, 2007, Standard Operating Procedure for Effluent Monitoring of Stormwater Discharges for Facilities Covered Under the MPDES Multi-Sector General Permit for Stormwater Discharges Associated Industrial Activities. Doc No. DEPLW0859.

Stenstrom, R.S., Clausen, J.C., Askew, D.R., 2002. Treatment of parking lot stormwater using a StormTreat system. Environmental Science and Technology 36 (20), 4441-4446.

Taylor, G.D., Fletcher, T.D., Wong, T.H.F., Breen, P.F., Duncan H.P., 2005. Nitrogen composition in urban runoff – implications for stormwater management. Water Research 39 (10), 1982-1989.

Van Dolah, R.F., Riekirk, G.H.M., Levisen, M.V., Scott, G.I., Fulton, M.H., Bearden, D., Sivertsen, S., Chung, K.W., Sanger, D.M., 2005. An evaluation of polycyclic aromatic hydrocarbon (PAH) runoff from highways into estuarine wetlands of South Carolina. Archives of Environmental Contamination and Toxicology 49, 391-396.

Vaze, J., Chiew, F.H.S., 2003. Study of pollutant washoff from small impervious experimental plots. Water Resources Research 39 (6), 1160-1170.

Westerlund, C., Viklander, M., 2006. Particles and associated metals in road runoff during snowmelt and rainfall. Science of the Total Environment 362(1-3), 143-156.

Williams, P.C., 2001. Implementation of near infrared technology. Near-Infrared Technology in the Agriculture and Food Industries, 145-171.

Wu, J.S., Homan, R.E., Dorney, J.R., 1996. Systematic evaluation of pollutant removal by urban wet detention ponds. Journal of Environmental Engineering, ASCE 122 (11), 983-988.

Ying, G., Sansalone, J.J., 2008. Partitioning and granulometric distribution of metal leachate from urban traffic dry deposition particulate matter subject to acidic rainfall and runoff retention. Water Research 42 (15), 2146-2162.

BIOGRAPHICAL SKETCH

Christina Herr graduated magna cum laude with her bachelor's degree in environmental engineering sciences with a minor in sustainability studies from the University of Florida in 2010. Christina received the degree of Master of Engineering in environmental engineering sciences from the University of Florida in August 2011. Her master's research was focused on experimentation of urban stormwater treatment unit operations and processes. She worked under the guidance of Dr. John J. Sansalone in the department of environmental engineering sciences. After graduation, Christina moved to Atlanta, Georgia to work in the Water Resources field.